Pulsatile flow dynamics maintain pulmonary arterial architecture

Stephen Spurgin,[1,2] Lauren Thai,[2] Tina Wan,[3,4] Christopher P. Chaney,[5] Mitzy A. Cowdin,[1] Suren V. Reddy,[2] M. Tarique Hussain,[2,6] Munes Fares,[2] M. Luisa Iruela-Arispe,[7] Thomas Carroll,[5] Andrew D. Spearman,[3] and Ondine Cleaver[1]*

[1]Department of Molecular Biology, University of Texas Southwestern Medical Center, 5323 Harry Hines Blvd., Dallas, Texas, USA 75390.

[2]Department of Pediatrics, Division of Cardiology, University of Texas Southwestern Medical Center, 5323 Harry Hines Blvd., Dallas, Texas, USA 75390.

[3]Department of Pediatrics, Division of Cardiology, Medical College of Wisconsin, Children's Wisconsin, Herma Heart Institute, Milwaukee, Wisconsin, USA.

[4]Cardiovascular Center, Medical College of Wisconsin, Milwaukee, Wisconsin, USA.

[5]Department of Internal Medicine and Division of Nephrology, University of Texas Southwestern Medical Center, 5323 Harry Hines Blvd., Dallas, Texas, USA 75390.

[6]Department of Radiology, University of Texas Southwestern Medical Center, 5323 Harry Hines Blvd., Dallas, Texas, USA 75390.

[7]Department of Cell and Developmental Biology, Northwestern Fienberg School of Medicine, Chicago, Illinois, USA 60611

*Corresponding author:

Ondine Cleaver

Department of Molecular Biology, University of Texas Southwestern Medical Center

5323 Harry Hines Blvd., NA8.300 Dallas, Texas 75390-9148, USA.

Phone: (214) 648-1647 Fax: (214) 648-1196

E-mail: ondine.cleaver@utsouthwestern.edu

Running title: **Pulsatile stretch drives mural thickness**

Word Count: 11,233 (all text inclusive)

Keywords: PDGFB, endothelial cell, mural cell, biomechanical force, hemodynamics, pulsatility, Glenn, single ventricle, congenital heart disease, rat, mouse

Non-standard Abbreviations and Acronyms

AV - arteriovenous

GSEA - Gene Set Enrichment Analysis

HAECs - human aortic endothelial cells

HPAECs - human pulmonary arterial endothelial cells

IF - immunofluorescence

IHC - immunohistochemistry

LPA - left pulmonary artery

L-SVC - left superior vena cava

NHLFs - normal human lung fibroblasts

PA - pulmonary artery

PASMCs - human pulmonary artery smooth muscle cells

PAVMs - microvascular pulmonary arteriovenous malformations

PDGFB - platelet derived growth factor B

PDGFR β - platelet derived growth receptor β

RPA - right pulmonary artery

SVC - superior vena cava

SV-CHD - Single ventricle congenital heart disease

vSMC - vascular smooth muscle cell

Abstract

Single ventricle congenital heart disease (SV-CHD) is a uniformly lethal condition requiring the Glenn surgery, which as a side effect eliminates arterial pulsatility and contributes to pulmonary vascular complications. In Glenn patients, we quantified pulsatility loss in each dimension of force (flow, pressure, and stretch) using cardiac catheterization and MRI. To model and investigate the individual impact of each dimension of pulsatility loss on the pulmonary vasculature, we applied isolated pulsatile and non-pulsatile mechanical stimuli to pulmonary arterial endothelial cells (ECs) in vitro. We found that each dimension of force triggered distinct transcriptional responses, revealing force-specific regulation of structural and signaling pathways. Pulsatile stretch uniquely stimulated EC secretion of PDGFB, a key driver of vascular smooth muscle cell (vSMC) recruitment. In a rat Glenn model, loss of pulsatility led to vascular wall thinning, confirming *in vivo* relevance. Our findings uncover a mechanistic link between endothelial stretch sensing and PDGFB-mediated EC-vSMC crosstalk, essential for maintaining pulmonary artery architecture. Clinically, these insights suggest that restoring or mimicking pulsatile forces may help preserve vascular integrity and prevent remodeling in SV-CHD patients.

Introduction

Globally, 1 in every 2000 babies is born with a heart that has a single functional ventricle (1). Surviving this congenital abnormality requires early and significant medical intervention. A single ventricle cannot perform the work of two for very long, nor can it direct an equal amount of blood flow to the lungs (low vascular resistance) and the body (high vascular resistance). For children with single ventricle congenital heart disease, survival depends on a series of remarkable surgeries: the Glenn and the Fontan. In the circulation created by these procedures, venous blood flows directly to the lungs without the support of a pumping ventricle, while the single functional ventricle supplies pulsatile flow to the rest of the body (2).

A frequent consequence of surgical replumbing of the vasculature in single ventricle patients is the development of a wide variety of vascular malformations: A) diffuse microvascular pulmonary arteriovenous malformations (PAVMs) in the Glenn stage and B) larger, tortuous collateral vessels in both Glenn and Fontan stages. It has been shown that the microvascular lesions that arise in the Glenn are reversible with restoration of the direct flow of liver blood to the lungs in the Fontan (albeit still lacking cardiac pulsatile flow). This has led to the “hepatic factor” hypothesis (3-5). However, interestingly, the proximal macrovascular collateral vessels in the Fontan do not regress (6, 7). Among the abundant potential pathogenic factors—chronic hypoxemia, chronic inflammation, and loss of direct hepatopulmonary blood flow (3, 5, 8)—a role for pulsatility has long been suggested (9-11), but never investigated at the mechanistic level.

Pulsatility, for its part, is a critical characteristic of arterial blood flow. Arteries—whether systemic, pulmonary, or umbilical—are *defined* by the presence of pulsatile blood flow, not by their color or oxygen content. The structure of the arterial wall—with thick

94 smooth muscle layer and elastic laminae—reflects the need to withstand the high
95 pulsations of arterial pressure and stretch. Veins, on the other hand, have less
96 hemodynamic pulsatility and a thinner smooth muscle layer (media) (12). Critically, the
97 histopathology of vascular malformations often reveals absent or patchy coverage of the
98 smooth muscle layer (13, 14). This mural insulation must be broken down to form new
99 connections between vessels. EC proliferation is a then a critical step in the pathogenesis
100 of vascular malformations (13). Once a connection is formed, the transmission of pulsatile,
101 arterial blood flow to venous vessels has been shown to induce “arterialization” (medial
102 thickening, intimal hyperplasia) of the venous vessels (15, 16), further highlighting the
103 relationship between arterial hemodynamics and the architecture of the vascular wall.
104 Although arteriovenous differences are most visually evident by their mural
105 coverage, the endothelial cells of arteries and veins are themselves distinct. They have
106 unique transcriptional and proteomic signatures (17), and unique developmental origins
107 (18, 19). The impact of cardiac pulsatility on the arterial side of the vasculature has been
108 appreciated in the early stages of vascularization (20)—however, the role of *pulsatility* in
109 maintaining arterial and venous endothelial identity and function *after* birth has received
110 very limited attention. Scientific investigation of EC mechanobiology has focused on other
111 physical forces, such as the cellular impact of low versus high shear stress, or of laminar
112 versus disturbed flow (21). Despite the clinical centrality of pulsatility, it remains an under-
113 investigated aspect of vascular biology.
114 ECs are remarkably sensitive to the physical forces transmitted by blood flow.
115 Endothelial mechanosensitive components include cell-cell adhesion molecules (integrins,
116 gap-junctions, cadherins), extracellular matrix (ECM) sensing components, ion channels,
117 and more (21, 22). The forces sensed by these molecular components are applied to ECs

118 in three dimensions: shear stress , pressure, and stretch (23). Each dimension of force
119 therefore exerts distinct stresses and deformations to ECs. Laminar shear stress (LSS) is
120 the frictional drag force that occurs along the inner (apical) surface of the vessel
121 endothelium (24). Stretch is the effect downstream of each heartbeat, as vessels widen
122 radially to accommodate an ejected volume of blood and their circumference expands (25).
123 Hydrostatic pressure is generated by ventricular contraction, and the driving force behind
124 stretch (26). Notably, ECs align parallel to the direction of LSS (blood flow) but
125 perpendicular to the direction of stretch (27)—further highlighting the need to consider
126 each dimension's impact separately. All three biomechanical forces have all been shown
127 to alter vascular ECM (28), as well as endothelial and smooth muscle transcriptional
128 programs (29, 30). However, the unique impact of pulsatility within each dimension of force
129 on vascular homeostasis remains a critical knowledge gap.

130 The endothelium and vascular smooth muscle communicate closely. Critically,
131 cross-talk between ECs and vSMCs is mediated by EC-secretion of platelet derived growth
132 factor B (PDGFB), which binds to PDGF receptor β (PDGFR β) on vSMCs, where it drives
133 proliferation and dictates mural cell coverage from large vessels down to the capillary level
134 (31, 32). Loss of Notch signaling in pericytes downregulates PDGFRB in vSMCs in mouse
135 models, leading to AVMs (33). Conversely, deleting PDGFB specifically from ECs has
136 shown remarkable dilation and arteriovenous shunting in the lungs of mice (34), and loss
137 of PDGFB has been observed in human vascular malformations (35). The question arises
138 as to whether different hemodynamic forces coordinate the maintenance of vascular
139 structure via EC responses to these forces.

140 Here, we investigate the biomechanical forces experienced by pulmonary ECs in
141 Glenn patients and identify pulsatility of blood flow as critical to maintenance of the lung

142 vasculature. We first use combined cardiac catheterization (cath) and cardiac magnetic
143 resonance imaging (MRI) to quantify and compare the pulsatility of force that is applied to
144 pulmonary arterial ECs in children with normal cardiopulmonary anatomy and in those with
145 Glenn circulation. After noting a clear loss of pulsatility in the Glenn pulmonary arteries, we
146 model those changes using cultured human pulmonary arterial endothelial cells (HPAECs)
147 to define the specific transcriptional programs driven by each individual dimension of force.
148 We demonstrate that pulsatile stretch in vitro, which mimics expansion of the arterial
149 vessel intima during cardiac ventricular systole, significantly impacts the transcriptional
150 landscape of ECs. Specifically, we show that pulsatile stretch stimulates ECs to secrete
151 PDGFB. In addition, using our previously published in vivo rat model of the Glenn surgery,
152 where pulmonary arteries (PAs) experience loss of pulsatile stretch, we demonstrate
153 significant reduction of PDGFB in PA ECs. Finally, we build on our recent work in a rat
154 model of the Glenn surgery(36), which showed early and progressive arteriovenous
155 shunting, to demonstrate significant thinning of pulmonary arterial vascular walls.
156 Together, our study identifies pulsatile stretch as a critical and underappreciated
157 dimension of arterial force that drives EC-secretion of PDGFB, promoting vascular smooth
158 muscle endowment and providing needed structural support for arterial vessels. Gaining
159 insight into the impact of *pulsatility* of hemodynamic force is a critical and novel approach
160 to understanding clinically relevant endothelial cell biology.
161
162
163

164 **Results**

165

166 **The Glenn shunt directs venous blood flow to pulmonary arteries**

167 Arterial vessels normally experience blood flow directly from a pumping cardiac
168 ventricle, adding pulsatility to the magnitude of hemodynamic forces (**Figure 1A**). By
169 reviewing the known characteristics of three distinct pairings of arteries and veins
170 (systemic, pulmonary, and umbilical), we note that pulsatile flow is a shared, definitional
171 quality of arteries (**Supplemental Figure 1**). Pulsatility is thus an inherent quality of blood
172 flow in arterial vessels. After a Glenn surgery, however, the pulmonary arteries no longer
173 receive blood flow directly from a pumping heart ventricle. Instead, pulmonary blood flow is
174 provided by the Glenn shunt: direct venous flow through the superior vena cava (SVC),
175 which is anastomosed to the pulmonary arteries (PA) (**Figure 1A'**). ECs that make up the
176 inner lining of pulmonary arteries downstream of normal cardiac vessel anatomy are
177 subjected to force in three dimensions: flow/sheer stress, pressure, and circumferential
178 stretch (**Figure 1B**) (23). Here, we assess these forces in the Glenn lung arteries.

179

180 **Pulsatility loss in three dimensions in Glenn patients**

181 To quantitatively determine the loss of pulmonary arterial pulsatility in patients with
182 Glenn anatomy, we used combined cardiac catheterization and cardiac MRI (cath/MRI) in
183 20 Glenn patients to obtain simultaneous data in all three dimensions of force: pressure,
184 flow, and circumferential stretch (**Figure 1B**). These data were compared to data obtained
185 in 20 age- and gender-matched patients with normal cardiopulmonary connections (see
186 patient demographics in **Supplemental Table 1**). First, as has long been observed
187 clinically, we observed pulsatility loss in the pulmonary arterial *pressure* of Glenn patients

188 (**Figure 1C, C'**). Similarly, we noted that the Glenn shunt leads to non-pulsatile shear
189 stress in the pulmonary arteries, as seen by a comparison of the pulmonary artery velocity
190 profiles in normal (**Figure 1D**) and Glenn (**Figure 1D'**) patients throughout the cardiac
191 cycle. Finally, we found that the circumference of proximal right pulmonary artery does not
192 expand repeatedly with each heartbeat in Glenn patients, demonstrating loss of pulsatile
193 *circumferential stretch* (**Figure 1E,E'**).
194
195 **Unique transcriptome for each dimension of pulsatile force**
196 ECs are highly responsive to mechanical force, and can react to differences in both
197 magnitude and direction of force.(37) Given the observed loss of pulsatility in Glenn
198 patients, we next investigated the relative impact of pulsatility within each dimension of
199 force on ECs.
200 Using our patient cath/MRI pulsatility data, we designed in vitro experiments that
201 model the pulsatility loss defined in Glenn patients. Each isolated, single dimension of
202 force was applied to cultured primary human pulmonary artery endothelial cells (HPAECs)
203 in a pulsatile and non-pulsatile manner. For pulsatile shear stress, we applied 0-15
204 dyn/cm^2 shear stress at 1 Hz, which mimics the frequency of a resting heart rate. For
205 pulsatile pressure, we modified the Ibidi equipment to expose HPAECs to columns of
206 media positioned to alternately provide 5 or 25 mmHg pressure, at 1 Hz, in the absence of
207 flow or stretch. For stretch, we used a Flexcell system to stretch HPAEC by 10% of their
208 baseline in a single axis (again at a frequency of 1 Hz). To assess stable transcriptional
209 changes between non-pulsatile and pulsatile conditions and thus improve in vivo relevance
210 of our findings, HPAECs were exposed to 48 hours of force or pulsatile force (**Figure 2A**).
211 To best mimic in vivo conditions in the years of the Glenn stage, pulsatile stretch was

212 compared to no stretch rather than continuous stretch, which does not happen in vivo. We
213 observed similar physical changes as have been reported previously: ECs align parallel to
214 the axis of flow and perpendicular to the axis of stretch and exhibit no alignment
215 preference under continuous or pulsatile pressure (**Figure 2B**).

216 The unique changes in cell shape in response to each axis of force highlight the
217 need to examine them individually. We first investigated the overall pathways that were
218 regulated by pulsatility. By Gene Set Enrichment Analysis (GSEA) of bulk RNAseq data,
219 we noted that each dimension of force drove changes in unique signaling pathways, and
220 that the impact of shear stress was the most distinct. Overall, in HPAECs, laminar flow
221 affected 19 unique pathways, stretch 10 unique pathways, and pressure 4 unique
222 pathways (**Figure 2C**). A wide range of pathway types were regulated, many related to
223 changes in structural cellular components, growth, or interaction of the cell with ECM
224 (**Figure 2D**). We note that mitogen-activated protein kinase (*Mapk*) and epidermal growth
225 factor receptor (*ErbB*, also known as *HER*) signaling were only induced by pulsatility of
226 flow, while Hedgehog and Notch signaling were only induced by pulsatility of stretch.
227 Pulsatile pressure did not uniquely regulate any obviously EC-related pathways, but did
228 upregulate the hypertrophic cardiomyopathy pathway.

229 In addition to these dimension-specific pathways, we find other pathways that are
230 influenced across multiple dimensions of force. We found 10 pathways upregulated by all 3
231 dimensions of force, and 17 pathways induced by two of the three dimensions. We note
232 that shear stress, stretch, and pressure all drove changes in the pathway “Regulation of
233 Actin Cytoskeleton.” However, an analysis of the leading-edge subset (the genes within
234 the pathway that are most significantly changed and thus responsible for the overall
235 significance of the pathway) revealed upregulation of different genes by each dimension of

236 force. For example, within the “Regulation of Actin Cytoskeleton” pathway, pulsatile
237 pressure shows *Actn1* and pulsatile flow yields *Map2k1*, while pulsatile stretch promotes
238 *Pdgfb*, *Arghef6,* and others (**Figure 2E**). Different dimensions of force therefore drive
239 different transcriptional changes that converge on similar pathways.
240
241 **Pulsatility does not alter arteriovenous genes in vitro**
242 To test the impact of each dimension of force on ECs, we next analyzed gene
243 transcription. Using the culture platforms shown in **Figure 3A**, we assessed bulk RNAseq
244 after application of single dimensions of pulsatile and non-pulsatile force. Strikingly, we
245 found very little overlap between genes enriched in ECs under different dimensions of
246 force, suggesting distinct responses to distinct forces. Importantly, we did not find
247 significant changes in baseline expression of common EC genes between the three
248 experimental set-ups (**Supplemental Figure 2**), indicating no basic alteration of
249 endothelial fate. Of the genes significantly regulated by pulsatility, 93.4% (1205/1290) were
250 driven by a single, unique dimension of force. Pulsatility of stretch accounted for over two-
251 thirds (888 genes, 68.9%) of these genes (**Figure 3B**). Only 59 genes were uniquely
252 induced by pulsatility of laminar flow, while 343 were uniquely induced by pulsatility of
253 pressure. We found less overlap in individual genes regulated by pulsatility than there was
254 in overall pathways. Twenty-two genes were regulated by pulsatility of both LSS and
255 stretch, 56 genes by stretch and pressure, and 5 by pressure and LSS.
256 Finally, we hypothesized that application of pulsatile force on cultured ECs would
257 induce greater expression of genes previously shown to be specific to arteries (17). We
258 asked whether the classical markers of arteriovenous (AV) EC differentiation were found in
259 these groups of genes. In cultured HPAECs, we found no dimension of pulsatility that

260 significantly affected the expression of a majority of developmental arterial (*Efnb2*, *Eng*,
261 *Sox17*, *Notch1, Jag1, Nrp1, Bmx)* or venous (*Ephb4*, *Emcn*, *Nr2f1*, *Nr2f2*/*Coup-TFII, Clu*)
262 driver genes (**Figure 3C**). Similarly, we found no significant changes arterial or venous
263 standard marker genes in rat Glenn arterial ECs compared to sham operated rats (data not
264 shown).

265 We next asked if there were genes specifically induced by pulsatile LSS, pressure
266 or stretch, when compared to the non-pulsative forces. After applying a p-value cut-off of
267 0.05 and fold change cut-off of 2, we found that pulsatile stretch drove a change in 44
268 genes, compared to 20 genes by pulsatility of flow, and 16 genes by pulsatility of pressure
269 (**Figure 3D-F**). Expression of these hits in data from other dimensions of force is shown in
270 **Supplemental Figure 3**. Genes upregulated under pulsatile LSS included many factors
271 involved in cell proliferation and immunity (red highlighted genes in **Figure 3D**), and genes
272 upregulated under pulsatile pressure included factors associated with the cytoskeleton and
273 RNA processing (red highlighted genes in **Figure 3E**). Gene expression was particularly
274 impacted by application of pulsatile stretch, with many factors involved in tissue
275 remodeling and inflammation being upregulated (red highlighted genes in **Figure 3F**) and
276 factors driving cell division and cell survival pathways (blue highlighted genes in **Figure**
277 **3F**).

278

279 **Identification of *Pdgfb* as a stretch-induced gene in pulmonary arterial endothelium**

280 As stretch accounted for the majority of pulsatility-regulated genes, we utilized
281 published single cell RNA sequencing of human lung tissue (LungMAP(38, 39)) to assess
282 the cell type-specific expression pattern of candidate genes. We reasoned that narrowing
283 the investigation to EC-specific genes might identify endothelial factors that sense flow and

284 normally respond by bolstering matrix or cellular components of the arterial media that
285 would increase resistance in proportion to hemodynamic load. *Mgp*, *Cx3cl1*, and *Pdgfb*
286 were highly expressed in a good proportion of ECs under stretch, but we noted high EC
287 specificity of the latter two genes (**Figure 4A**). Analysis of the expression of these ligands
288 and their receptors (*Cx3cl1R* and *Pdgfrb*, respectively) underscored the pulsatility-induced
289 crosstalk between ECs and immune cells (for *Cx3cl1*) and between ECs and perivascular
290 cells (for *Pdgfb*) (**Figure 4B-D**). As PDGFB is i) well known to promote smooth muscle cell
291 proliferation and recruitment (31), ii) a key component of the GSEA for ECs under stretch
292 (**Figure 2**), and iii) a significant hit in their differential gene expression (**Figure 3**), we
293 investigated further its role in pulmonary vessels.
294
295 **Pulsatile stretch uniquely drives EC PDGFB secretion**
296 We next asked if stretch-induction of PDGFB expression was specific to ECs or also
297 present in other cellular components of the vessel wall (vascular smooth muscle or
298 fibroblasts). We applied cyclic 10% stretch to HPAECs from two different patients, human
299 aortic endothelial cells (HAECs), human pulmonary artery smooth muscle cells (PASMCs),
300 and normal human lung fibroblasts (NHLFs). We found that pulsatile stretch robustly
301 induced secretion of PDGFB exclusively from endothelial cell lines (**Figure 4E**). As
302 PDGFB is known to be induced by flow (40), we compared PDGFB secretion from ECs
303 under continuous flow (mimicking venous condition) to pulsatile stretch (mimicking arterial
304 condition). Induction of PDGFB by pulsatile stretch was 5x higher than the induction by
305 laminar, continuous flow (**Figure 4F**).
306 We next assessed whether we could detect EC secretion of PDGFB in human
307 patients following similar pulsatile stretch-induction. We anticipated that we would not be

308 able to detect a change in the circulating blood, as PDGFB is secreted basally to the
309 perivascular space, not apically into the blood stream, as shown previously (41). To do
310 this, we tested the blood of patients with either normal or Glenn anatomy. As expected,
311 analysis of PDGFB expression in plasma obtained from the pulmonary artery and
312 pulmonary vein revealed significant variation in local PDGFB expression in both normal
313 and Glenn patients that could not be correlated with pulmonary arterial pulsatility (**Figure**
314 **4G**).
315
316 **Decreased PDGFB expression in pulmonary arteriole ECs of the Glenn rat model**
317 Given the finding that stretch induces PDGFB secretion from pulmonary ECs, we
318 utilized our animal model of the Glenn surgery to test whether arteries receiving non-
319 pulsatile flow exhibited decreased endothelial PDGFB synthesis in vivo. We performed an
320 end-to-end anastomosis of the left SVC (L-SVC) and the left pulmonary artery (LPA)
321 (**Figure 5A, A'**). This mimics the Glenn surgery, directing only non-pulsatile venous blood
322 flow from the head and upper extremity into the pulmonary artery. As previously described,
323 these rats develop hypoxemia secondary to intrapulmonary arteriovenous shunting.(36)
324 The hypoxemia develops rapidly (after two weeks) and is progressive (to six months (36)).
325 To test whether arteries receiving non-pulsatile flow exhibited decreased PDGFB
326 synthesis in their ECs, we focused on the distal lung arterioles—in the vicinity of where
327 AVMs form in our patients, and where EC-specific expression of PDGFB is highest by
328 single cell RNAseq (**Figure 4A**). To localize these arterioles and the PDGFB expression
329 within the ECs, we used immunofluorescent staining with antibodies recognizing the
330 endothelial junctional marker VE-cadherin (CDH5), the vascular smooth muscle marker
331 alpha smooth muscle actin (aSMA) and the PDGFB protein (42). We found significant

332 reduction of endothelial PDGFB in arterioles of the Glenn rat (**Figure 5B**). Critically, we
333 also noted loss of smooth muscle surrounding these distal arterial vessels in the Glenn.
334 Quantification of PDGFB IF signal from 5 arterioles each from 3 sham and 3 Glenn-
335 operated left lungs revealed a significant decrease in endothelial PDGFB expression in the
336 Glenn arterioles, but not in alveolar capillary ECs (**Figure 5C**).
337
338 **Rat Glenn displays reduced pulmonary arterial smooth muscle**
339 We hypothesized that a further consequence of reduced PDGFB in pulmonary ECs
340 under the non-pulsatile Glenn hemodynamics would be loss of the smooth muscle layer.
341 We analyzed sagittal sections of the left lung of 9 Glenn rats and 5 sham-operated rats
342 and performed immunohistochemistry (IHC) for smooth muscle actin (SMA). Strikingly, we
343 found a significant decrease in arterial smooth muscle thickness (SMA+ cells) (**Figure 6A,**
344 **B**), while venous smooth muscle thickness remained unchanged (**Figure 6C**). We
345 observed this reduction in vascular wall thickness in both the largest proximal arteries
346 (**Figure 6A-C**), as well as the distal arterioles, less than 0.1 mm in diameter (**Figure 6D-**
347 **G**).
348
349

Discussion

In this study, we identify hemodynamic pulsatility as critical to maintenance of the pulmonary arterial architecture (**Figure 7**). We show that in patients with Glenn circulation the shunted pulmonary blood flow—from the SVC directly to the PA—exerts no pulsatile stretch on the pulmonary artery. Using transcriptomic analysis, we show that cultured pulmonary arterial ECs exposed to each dimension of force elicit distinct molecular signatures. We find that pulsatile stretch induces significant endothelial secretion of PDGFB, known to mediate recruitment of vSMCs to blood vessels (31, 32). As lung biopsies from living patients were not obtainable, our rat model of the Glenn circulation allowed us to investigate the effect of pulsatility loss in vivo. Using this animal model, we show that non-pulsatile, venous flow within an arterial vessel, results in loss of PDGFB protein from ECs and concomitant thinning of the vascular mural wall. Our complementary in vitro and in vivo findings identify a new target signaling pathway for novel therapeutic approaches to treat the diverse vascular malformations that occur in Glenn patients.

Despite clinical appreciation of the fact that Glenn patients experience venous-type, non-pulsatile blood flow in pulmonary arteries, and even though pulsatility loss was the first hypothesized mechanism for Glenn PAVMs (43, 44), pulsatility loss has never been formally documented in three dimensions. Until now, studies comparing surgical outcomes of Glenn patients have only occasionally been able to report some dimensions of pulsatility loss (9, 45), although most studies report none (46-52). This clinical knowledge gap has limited our understanding of the impact of pulsatility within these patients. Our use of combined cardiac catheterization and cardiac MRI (cath/MRI) ensures that these

interdependent forces are measured simultaneously, providing with high temporal accuracy the first complete 3D view of pulsatility loss in the Glenn pulmonary arteries.

Our pulsatility metrics merit two points of discussion. First, we utilize flow velocities as a surrogate for wall shear stress (WSS)—the direct hemodynamic force applied to the endothelium. As WSS depends directly on the velocity gradient, velocity is a reasonable approximation for this investigation. Given the limited availability and accuracy of WSS measurements with cardiac MRI, use of velocity instead of the highly regionally variable WSS supports an easier and more rapid clinical application. Second, the relationship between pressure and stretch (vascular compliance) is not directly tested in our study. This will be a critical area of investigation in the future, to answer the question of how much pulsatility (of flow, pressure, or stretch) is present in the distal lung.

Indeed, estimating the magnitude of pulsatile forces across the pulmonary vascular tree is difficult. Arterial pulsatility in normal patients is likely significantly diminished as it reaches distal capillaries. Dynamic measurement of distal pulsatility of stretch in sub-millimeter vessels in vivo is technically challenging and could not be directly assessed by our methods. In a normal compliant vessel, proximal stretch acts as a capacitor, absorbing and lessening distal pulsatility—a phenomenon termed the ‘windkessel effect’ (53). This model suggests a reduction of pulsatility in the normal distal microvasculature. Our proposed mechanism—that pulsatile stretch of ECs stimulates PDGFB followed by smooth muscle coverage—is supported by the observation that normal arterial smooth muscle thins as vessels branch further into the lung (12). PDGFB was originally described as flow responsive (40), and later as stretch responsive (54), although in our in vitro work stretch elicited 5-fold more PDGFB secretion than flow. The opportunity now arises to characterize the relative contribution of shear and stretch to PDGFB secretion in these distal vessels.

397 We also recognize that the presence of respiratory-driven alveolar stretch (at a much lower
398 frequency) may also contribute to distal pulsatility (55, 56). In all, these studies underscore
399 the importance of pulsatility throughout the entire arterial network and bring up new
400 questions about the impact of biomechanical cues on the lung vasculature.

401 How do ECs sense hemodynamic forces in lung vessels? We previously
402 hypothesized that endothelial cilia could be involved in sensing pulsatility of flow (57) but
403 disproved this possibility in the mammalian lung as pulmonary ECs are devoid of primary
404 cilia (58). Endothelial mechanosensitive components have been well described and are
405 present on lung ECs. Notch, Cdh5, and many other cell-surface proteins, ECM, and
406 cytoskeletal elements are all required for proper sensing of flow or stretch (23). In
407 particular, the protein complex of PECAM1, CDH5, VEGFR2/3, and PLXND1 plays a
408 critical role in force-sensing, while proteins like LPHN2 and others coordinate downstream
409 responses (59). In our data, we see significant upregulation of *Plxnd1*, as well as near two-
410 fold increases in *Cdh5, Kdr,* and *Lphn2* (data not shown) under pulsatile pressure
411 conditions, but not pulsatile stretch or LSS —suggesting a possible role for pulsatile
412 pressure in priming the endothelium to respond to force. Our study thus highlights the
413 need to consider each dimension of force separately, as we continue to evaluate the role
414 that pulsatility plays in the maintenance of the normal vascular architecture.

415 One key question is how loss of pulsatility impacts arteriovenous fate in Glenn
416 vessels. Our studies show that the Glenn shunt supplies venous-type hemodynamic forces
417 to an artery, as blood flow pulsatility is lost following surgical intervention. The observed
418 outcome of this change in biomechanical forces is that the artery becomes structurally
419 more like a vein, in that its vascular wall is significantly diminished in thickness. While
420 enhancement of arterial EC markers by pulsatility of LSS has been observed previously in

421 vitro (20), in our studies, we did not find enhancement of classic markers of arterial EC
422 identity under pulsatile conditions (in any dimension of force), nor did we find shifts in
423 arteriovenous identity in our rat Glenn model (data not shown). It is possible—if unlikely—
424 that this difference is due to the highly laminar flow provided by the Ibidi system in our
425 work, compared to the more turbulent flow in the cone-disc viscometer used in the prior
426 study. Separately, microvessels exposed to arterial anastomosis have been observed to
427 increase vSMC coverage (60), however changes in EC arteriovenous identity were not
428 noted. These observations support our conclusion that pulsatility drives the arterial
429 vascular structure as a whole (EC + surrounding mural cells), rather than the shifting the
430 expression of developmentally-regulated markers of arteriovenous EC identity.

431 Growing evidence has pointed to a potential venous origin of AVMs (61, 62), while
432 our study focused on upstream impacts within lung arteries and upregulation of endothelial
433 PDGFB. Endothelial deletion of *Pdgfb* (using Cdh5-CreERT2) in mouse leads to vascular
434 malformations in mouse lungs, while arterial-specific ablation (using Bmx-Cre) does not
435 (34). However, we note that in these studies, ablation was induced over a short timeframe
436 (1 week) and only retinal arteries were assessed. It will be important to examine how
437 arterial loss of *Pdgfb* over a longer timeframe, like that experienced by patients and Glenn
438 rats, impacts downstream PAVMs. Hence, the mechanisms and time course of how
439 upstream biomechanical cues impact arterial ECs and the downstream endothelium of
440 capillaries and veins, and whether there are organotypic effects, remains to be seen.

441 Other cells of the vascular wall, such as vSMCs, also certainly sense biomechanical
442 forces. VSMCs experience stretch similar to ECs, but not LSS as they are not in direct
443 contact with blood flow. Interestingly, vSMCs respond differently to stretch than ECs,
444 aligning perpendicular to stretch in vivo, rather than parallel like ECs (63). In our study and

445 in publicly available single cell RNA sequencing from human lung, we also find that smooth
446 muscle cells do not secrete PDGFB. We note that vSMCs from rat Glenn do not show
447 changes in standard vSMC genes such as *myh11, tagln, myocd, cnn1*, and *pdgfrb* (data
448 not shown). This does not rule out, however, the possible contribution of vSMCs to the
449 ECM, especially regarding the alterations in pulmonary vascular resistance and vessel
450 stiffening that so critically drive patient outcomes. Future studies will be necessary to
451 investigate the responses of vascular smooth muscle to pulsatile stretch.

452 While we focused here on *Pdgfb*, we also note that under pulsatile flow there is a
453 significant upregulation of *Col1a2,* a major component of vascular wall. Loss of *Col1a2* is
454 associated with vasculopathy and aortic dilation (64), suggesting that pulsatility of stretch
455 likely drives other EC contributions to the structure of the arterial wall—and arterial
456 vascular identity—beyond the recruitment of vSMCs. Regulation of the ECM is a logical
457 complimentary function of pulsatility, as the scaffold for the vSMCs and the internal elastic
458 lamina of the largest arteries are unique features of overall arterial structure. Our work thus
459 highlights a distinction between the traditional markers of arteriovenous endothelial identity
460 (EC-centric) and arteriovenous vascular identity (the overall structure of the vessels
461 cellular layers and ECM).

462 In addition, we also noted the upregulation of CX3CL1 in pulsatile-stretched
463 HPAECs. CX3CL1 is a well-known chemokine that increases leukocyte recruitment and
464 adhesion to ECs (65, 66). Multiple other chemokines (CCL2, CCL14) are regulated by
465 pulsatility in our in vitro system. The role of the immune system in the vascular
466 complications of Glenn circulation is a wholly unappreciated factor; however, previous
467 work in hereditary AVMs identified accumulation of leukocytes in brain AVMs and skin

468 telangiectasias (67-69). Collectively, these findings suggest that pulsatile stretch may
469 impact EC-leukocyte crosstalk in pathogenesis of vascular malformations.

470 Translation of our findings will depend on the relative role of pulsatility in the
471 pathogenesis of the different vascular malformations that arise in the Glenn lung. They are
472 highly diverse, and include both large “collateral” vessel formation proximally, as well as
473 microvascular arteriovenous malformations distally (7). As patients can present with
474 primarily proximal, primarily distal, or both types of malformations, it is highly likely that the
475 pathogenesis of these lesions is multifactorial, with both common and distinct elements. As
476 previously noted, there is 50 years of evidence that a “hepatic factor” is the primary
477 pathogenic factor for distal microvascular PAVMs. However, we suggest it is not likely the
478 only factor. An argument for the hepatic factor as the primary pathogenic factor is the
479 observation that distal PAVMs are reversible in the Fontan stage, which restores direct
480 hepatopulmonary venous blood flow but not normal pulsatility. However, the proximal
481 collateral vessels do not resolve in the Fontan, pointing to a critical role for pulsatile flow in
482 vascular architecture. In our study, we observe thinning of vSMCs both proximally and
483 distally in the animal model and therefore suggest that pulsatility may be a primary factor in
484 the generation of proximal collateral vessels and an exacerbating factor in the
485 development of distal PAVMs.

486 The relative contribution of pulsatility and hepatic factor to the pathogenesis of distal
487 AVMs can be assessed by comparing the time of onset in the Glenn and other clinical
488 scenarios. In Glenn patients (no hepatic factor, no pulsatility), AVMs can develop in
489 months (7, 70-72). However, in a rare subset of heterotaxy patients (no hepatic factor,
490 normal pulsatile flow) (73-76), AVMs form more slowly. In these latter patients, who have
491 interrupted inferior vena cava (strongly suggesting left isomerism heterotaxy syndrome

492 (77)), the hepatic veins can (rarely) drain directly to the left atrium in an otherwise normal
493 biventricular heart with intact atrial and ventricular septa. In this scenario (pulsatile
494 pulmonary blood flow, diversion of hepatic venous blood from the lungs), distal PAVMs can
495 take years or even decades to appear (73-76). This suggests that loss of pulsatility
496 critically accelerates the pathogenesis of distal pulmonary AVMs but is not sufficient to
497 induce them.

498 Thus, while loss of pulsatility may not be the defining factor that leads to distal
499 pulmonary AVMs in the Glenn stage, they are correlated in our rat model. Our
500 immunohistochemical and immunofluorescent evaluation in the Glenn rat model shows
501 dramatic changes of both proximal and distal pulmonary arterial mural cell recruitment
502 Currently, descriptions of dilated distal vessels in the Glenn population exist (78-80);
503 however, there has been no histological analysis of proximal pulmonary arteries. Work in
504 Fontan patients, however, has shown thinning of the proximal pulmonary arterial media
505 (81, 82). The persistence of thin media (proximally, where collaterals form) even as distal
506 PAVMs resolve in the Fontan stage suggests a critical role for pulsatility in maintenance of
507 proximal vascular architecture. We suggest that pulsatility loss is therefore likely a
508 common pathogenic factor in the development of both proximal collateral vessels and
509 distal AVMs.

510 In summary, we show that the pulsatility of hemodynamic forces in blood vessels is
511 sensed by the endothelium uniquely in each dimension of force. Our data support a model
512 whereby pulsatile stretch induces endothelium to secrete PDGFB, signaling for support
513 from vascular smooth muscle. Indeed, the architecture and cellular composition of the
514 vessel wall change significantly upon loss of pulsatility in the Glenn, with thinning of the
515 vascular wall, thereby shifting the arterial vascular wall structure toward that of a vein,

516 likely impacting downstream endothelium. Together, this work underscores the critical
517 importance of proper blood flow dynamics for the stability of vascular structure and
518 function. In addition, it points to biomechanical signaling pathways as potential novel
519 targets for therapeutic intervention in patients with pulsatility loss, such as in the Glenn
520 circulation. We seek to better understand and address the mechanistic underpinnings of
521 vascular defects that occur during single ventricle palliation and anticipate that our data on
522 pulsatility will provide the foundation for improving clinical outcomes for children that
523 undergo these necessary surgeries.
524

525 **Methods**

526

527 **Data Availability**

528 All sequencing data that support the findings of this study have been deposited in the
529 National Center for Biotechnology Information Gene Expression Omnibus (GEO) and are
530 accessible through the GEO Series accession number GSE298790. All other relevant data
531 are available from the corresponding author on request.

532

533 **Combined cardiac catheterization and cardiac MRI**

534 Combined cardiac catheterization and MRI was performed on a Philips XMR setup
535 (Phillips Ingenia Evolution, Best, Netherlands).(83) This consists of a 1.5T MRI-scanner
536 and a BV Pulsera or Allura Clarity or Ingenia (Philips) cardiac X-Ray unit. An appropriate
537 size balloon wedge catheter (Arrow Intl., Reading, PA) and receiver coil were used
538 depending on the weight of the patient.

539

540 All studies were conducted under general anesthesia based on clinical need. Patients
541 were recruited and data was recorded in sequence of the patient's referral for the
542 procedure under University of Texas Southwestern IRB-approved study (STU 032016-009)
543 in 2023 - 2024. All Glenn patients with a single functional ventricle were considered for
544 inclusion in the study. Patients were excluded if they had pulmonary blood flow in addition
545 to the flow provided by the Glenn anastomosis. Both male and female patients were
546 included in the study (see Supplemental Table 1).

547

548 Pulsatility was assessed by pulse difference, which was defined as the difference between
549 maximum and minimum value for each parameter of force. Pulsatility index was not
550 selected due to the potential for obscuring differences between patients (see Supplemental
551 Table 2). For each 2D cross-section of the right pulmonary artery obtained, we obtained a
552 mean velocity (averaged over the cross section of the vessel). This data is obtained over 1
553 to 2 minutes 'free-breathing' using phase contrast velocity-encoded cine MRI. Sequence
554 parameters included 40 cardiac phases, TE/TR = 2.7/4.4 ms (TE = echo time, TR =
555 repetition time), with two signal averages, 1.5-2mm × 1.5-2mm × 6-8 mm resolution,
556 SENSE acceleration factor = 2, with the velocity encoding gradient set to 25% above the
557 expected maximum velocity in each vessel. Vendor-provided background phase correction
558 was used. Artificial intelligence-assisted segmentation using Circle (Circle Cardiovascular
559 Imaging, CVI42, v6.1.2) was performed to obtain the maximum and minimum area, from
560 which an idealized circumference was calculated. Pressure tracings were obtained on a
561 standard Siemens Sensis Hemodynamic recording system (Siemens Healthineers,
562 Munich, Germany), using a 5- or 6-French Arrow, Balloon Wedge-Pressure Catheter
563 (Teleflex Medical Headquarter International, Ireland) located in the proximal right branch
564 pulmonary artery.
565
566 **In vitro cell-based assays of pulsatile force**
567 Pulsatile force was applied to confluent monolayers of human pulmonary artery endothelial
568 cells (HPAECs, Lonza) for 48 hours under each condition. Pulsatile (1 Hz, 15 dyn/cm^2) and
569 continuous (15 dyn/cm2) shear was applied using the Ibidi system (Ibidi USA, Wisconsin).
570 Pulsatile (25-5 mm Hg) and continuous (25 mm Hg) pressure was applied using a custom
571 modification to the Ibidi system whereby cells were alternately (1 Hz) exposed to columns

572 of culture media to deliver the desired hydrostatic pressure. Pressure readings were tested
573 and confirmed the using the Siemens Sensis Hemodynamic recording system listed
574 above. Pulsatile stretch was applied using Uniflex plates (1Hz, 1 hr of 3% stretch for
575 acclimation followed by 47 hrs of 10% stretch) as a part of the Flexcell FX-6000 system
576 (Flexcell International, Burlington, NC). Ibidi channels were pre-coated with the proprietary
577 Ibi-treat to promote cell adhesion, and Flexcell uniflex plates were coated with 0.1% gelatin
578 to promote cell adhesion.
579
580 All experiments utilized at least three biological replicates, using separate aliquots of
581 HPAECs from two different donors. RNA was extracted using RNeasy Plus kit (Qiagen)
582 prior to bulk RNA sequencing. Library generation and bulk RNA sequencing was carried
583 out by the McDermott Next Generation Sequencing core facility at UT Southwestern
584 Medical Center, using an Illumina NextSeq 2000. Processed sequencing data (using
585 iGenomes annotations) was provided by the core, and a TPM cutoff of 10 was applied (if
586 any test condition resulted in a gene's TPM >10, the gene was included in our analysis).
587 PCA plots of each condition are shown in **Supplementary Figure 4**.
588
589 For pathway analysis, we performed gene set enrichment analysis was performed for sets
590 curated in MsigDb (PMID 26771021) using with fgsea (BioRxiv
591 https://doi.org/10.1101/060012) Bioconductor package. To simultaneously account for both
592 the magnitude and significance of the measured effects, genes were ranked by the
593 quotient of log fold-change and adjusted P-value.
594
595 **Human Lung Single Cell RNA sequencing**

596 The LungMAP Human Lung CellRef atlas was utilized via the online portal at
597 www.lungmap.net. (38, 39) This dataset includes 148 normal human lung samples from
598 104 donors, including child, adolescent, and adult tissue. Tissue types include
599 parenchyma, trachea, bronchi, bronchus, and small airways. 347,970 cells from the
600 dataset were included in our analysis. Both ShinyCell and cell x gene were utilized for
601 visualization of cell-specific gene expression. Dataset ID: LMEX0000004396.
602
603 **Measurement of PDGFB secretion in vitro**
604 Cultured HPAECs, human arterial endothelial cells (HAECs, Lonza), human pulmonary
605 artery smooth muscle cells (PASMCs, Lonza), and normal human lung fibroblasts (NHLFs,
606 Lonza were plated onto Flexcell uniflex plates (pre-coated with collagen I). Each cell line
607 was grown in the recommended cell culture media, obtained from Lonza: HPAECs and
608 HAECs were grown in EGM-2, PASMCs in SmGM-2, and NHLFs in FGM-2. Cells were
609 grown to confluency then subjected to pulsatile stretch for 48 hours as above. Media was
610 collected and PDGF-BB was measured by ELISA (R+D systems DY220). For comparison
611 to endothelial cells under flow, media was obtained from confluent HPAECs in 6 well
612 plates under continuous flow at 15 dyn/cm^2 shear stress in a rotational flow apparatus
613 (Thermo Scientific Model No: 88881101).
614
615 For measurement of transpulmonary gradient of PDGF-BB (here termed PDGFB) in
616 human plasma, samples were obtained directly from Glenn and heart transplant patients in
617 the course of regularly indicated cardiac catheterization. Patients were consented for the
618 IRB approved study (University of Texas Southwestern IRB: UTSW-2020-0047). Samples
619 were obtained from the pre-capillary blood (right pulmonary artery) and the post-capillary

620 blood (right pulmonary wedge position, with the catheter in the distal pulmonary artery with
621 balloon inflated and the sample drawn through the end hole) in each patient. Nature of
622 each sample as pre- or post-capillary was then confirmed by prompt measurement of
623 oxygen saturation, and only fully oxygenated samples were used for the analysis. All
624 samples were obtained in K2-EDTA purple-top tubes, placed on ice, and promptly spun
625 down for plasma isolation. Samples were stored at -80°C up to 2 years maximum prior to
626 measurement by ELISA as above.
627
628 **Surgical Rat Model of Glenn Circulation**
629 The rat surgical model of Glenn circulation is described in detail previously.(36) Briefly, we
630 performed an end-to-end cavopulmonary anastomosis between the left superior vena cava
631 (L-SVC) and the left pulmonary artery (LPA). This was previously shown to result in
632 progressive impairment (beginning by two weeks) in oxygenation in tandem with the
633 development of intrapulmonary arteriovenous shunts as detected by both bubble
634 echocardiography and microsphere injection.
635
636 Adult Sprague–Dawley rats (male and female, 6–12 weeks of age) were used for all
637 experiments (Taconic). All rats were housed in the Biomedical Research Center at the
638 Medical College of Wisconsin with access to standard chow diet (PicoLab Lab Diet, 5L0D),
639 water ad libitum, and maintained in a 12-hour light/dark cycle. All surgical procedures were
640 performed under isoflurane anesthesia (1%–3%). All experimental protocols were
641 approved by the Medical College of Wisconsin Institutional Animal Care and Use
642 Committee prior to initiation of experimental protocols (Animal Use Agreement #7731).
643

644 **Tissue Preparation and Immunohistochemistry (IHC) /Immunofluorescence (IF)**

645 Lungs were harvested at 2 and 6 months after surgery for these experiments. Lungs were
646 inflated to 10 mmHg for 10 minutes with 10% neutral buffered formalin to promote normal
647 alveolar architecture in sections, followed by overnight fixation in 10% neutral buffered
648 formalin. Formalin-fixed, paraffin-embedded sections were prepared using the left lung of
649 the Glenn and sham operated animals. IHC staining was done for SMA (Abcam, ab7817)
650 using the Leica Bond Rx automated staining platform with Leica BOND Polymer Refine
651 Detection kit (Leica, DS9800) per manufacturer instructions, using standard labeled-
652 streptavidin-biotin detection with secondary antibody (Jackson Immuno Research Labs,
653 Biotinylated donkey anti-mouse 1:500, #715-066-151), streptavidin HRP (Vector
654 Laboratories, #SA-5004), and DAB chromogen (BioCare, BDB2004).

655

656 Slides were scanned using Hamamatsu HT whole slide scanner (Hamamatsu, USA) and
657 analyzed with QuPath (Edinburgh, V0.5.1). The file names were randomized and blinded
658 prior to analysis. Due to the possibility of changes in vessel size between sham and Glenn-
659 operated rates, measurements were taken from the most proximal pulmonary arteries and
660 veins to ensure a valid comparison between samples. Arteries were differentiated from
661 veins in consultation with a trained pathologist, by their classic histological characteristics
662 and anatomical proximity to the mainstem bronchi. Slides were not utilized for
663 measurement if no major bronchi or large vessels could be identified. Measurements were
664 taken only in areas where the thickness was uniform and the endothelial cells formed a
665 clear monolayer, to avoid artifactual error from the angle of the slice.10 measurements of
666 each large vessel (artery or vein, Glenn or sham-operated) were obtained, and the mean
667 measurement value was used for analysis.

We used IF staining and confocal microscopy to identify distal vessels for quantification of endothelial PDGFB protein and perivascular smooth muscle. Lung sections were prepared as above. Sections were permeabilized for 10 min in 0.2% Triton X-100 in PBS, then subjected to antigen retrieval with R-buffer B in a 2100 Retriever (Electron Microscopy Sciences). Slides were blocked with CAS-block (Invitrogen), and primary antibody incubations were carried out at 4°C overnight. Primary antibodies were as follows: VE-cadherin/CDH5 (R+D systems, AF1002, 1:100), PDGFB (Santa Cruz, sc-365805, 1:100), and SMA-APC (Abcam, ab225143, 1:400). Imaging was performed on a Nikon CSU-W1 dual-camera inverted spinning-disc confocal microscope. Vessels were chosen as <50 μm and >20 μm in diameter, with a clear lumen and apical VE-cadherin staining visible. Images were analyzed in Fiji as follows: the percentage of the circumference of each vessel covered by SMA staining was calculated, and a mask was made of the pixels positive for SMA staining in the sub-endothelial region and the mean pixel intensity of those pixels was calculated.

Statistical Analysis

Sample sizes were based on patient availability and standards in the field. Data were both analyzed and plotted in Graphpad PRISM 10.2.3. Descriptive statistics (mean, standard deviation, median, min, and max) were employed for summarizing demographic, hemodynamic, and clinical variables. Statistical tests (indicated in the relevant methods sections and figure legends) utilized were the parametric unpaired Student's *t*-test and the one-way ANOVA with Tukey's multiple comparisons test. Statistical significance is noted as follows: ns = $p > 0.05$; * = $0.01 < p < 0.05$; ** = $0.001 < p < 0.01$; *** = $0.0001 < p < 0.001$; **** = $p < 0.0001$. Superplots were made with individual colors representing biological

692 replicates (individual rats), and the mean of the averages of each biological replicate is
693 shown (84). Cell images were analyzed in FIJI. Figures and models were made using
694 Microsoft PowerPoint, data were partially analyzed in Microsoft Excel, and text was written
695 in Microsoft Word.
696

ACKNOWLEDGEMENTS

We are grateful to the entire Cleaver Lab for useful discussions and reading of the manuscript. We thank Denise Marciano for the use of her lab's Flexcell apparatus. We thank the UT Southwestern Medical Center (UTSW) Quantitative Light Microscopy Core Facility (Marcel Mettlen, Ph.D.) for training/assistance. The results here are in part based upon data generated by the LungMAP Consortium and downloaded from (www.lungmap.net), on March 15, 2025. The LungMAP consortium, the Human Tissue Core (U01-HL144861), and the LungMAP Data Coordinating Center (U24-HL148865) are funded by the National Heart, Lung, and Blood Institute (NHLBI).

Author contributions

Conceptualization: S.S., T.H., M.F., M.L.I.A., O.C.; Methodology: S.S., T.H., M.F., S.R., A.D.S., O.C.; Investigation: S.S., L.T., T.W., S.R., O.C.; Resources: S.S., T.W., A.D.S., T.C., O.C.; Data curation: S.S., M.A.C., L.T., T.H.; Writing - original draft: S.S., O.C.; Writing - review & editing: S.S., T.H., M.L.I.A., A.D.S., O.C.; Visualization: M.A.C., S.S.; Supervision: S.S., O.C.; Project administration: S.S., O.C.; Funding acquisition: S.S., T.C., A.D.S., O.C.

Funding

This research was supported in part by grants from the American Thoracic Society/Alveolar Capillary Dysplasia (ACDMPV) Research Grant (23-24PACDA12 to S.S.); National Heart Lung and Blood Institute (1R01HL-175575 to M.L.I.A., K08HL157510 to ADS, HL113498 and HL126518 to O.C.); the National Academy of Science, Engineering,

721 and Medicine Ford Foundation Dissertation Fellowship (M.A.C.); National Institutes of
722 Health (R01DK127634, RC2 DK125960 to T.C.) and Cancer Prevention Research Institute
723 of Texas (RP220201 to T.C.); and the Foundation Leducq grant (21CVD03 to M.L.I.A.,
724 O.C.). Open Access funding provided by University of Texas Southwestern Medical
725 Center. Deposited in PMC for immediate release.
726

833 **REFERENCES**
834

835 1. Liu Y, Chen S, Zuhlke L, Black GC, Choy MK, Li N, et al. Global birth prevalence of
836 congenital heart defects 1970-2017: updated systematic review and meta-analysis of
837 260 studies. *Int J Epidemiol.* 2019;48(2):455-63.
838 2. Rychik J, Atz AM, Celermajer DS, Deal BJ, Gatzoulis MA, Gewillig MH, et al. Evaluation
839 and Management of the Child and Adult With Fontan Circulation: A Scientific Statement
840 From the American Heart Association. *Circulation.* 2019:CIR0000000000000696.
841 3. Srivastava D, Preminger T, Lock JE, Mandell V, Keane JF, Mayer JE, Jr., et al. Hepatic
842 venous blood and the development of pulmonary arteriovenous malformations in
843 congenital heart disease. *Circulation.* 1995;92(5):1217-22.
844 4. Pike NA, Vricella LA, Feinstein JA, Black MD, and Reitz BA. Regression of severe
845 pulmonary arteriovenous malformations after Fontan revision and "hepatic factor"
846 rerouting. *Ann Thorac Surg.* 2004;78(2):697-9.
847 5. McElhinney DB, Kreutzer J, Lang P, Mayer JE, Jr., del Nido PJ, and Lock JE. Incorporation
848 of the hepatic veins into the cavopulmonary circulation in patients with heterotaxy and
849 pulmonary arteriovenous malformations after a Kawashima procedure. *Ann Thorac*
850 *Surg.* 2005;80(5):1597-603.
851 6. Kavarana MN, Jones JA, Stroud RE, Bradley SM, Ikonomidis JS, and Mukherjee R.
852 Pulmonary arteriovenous malformations after the superior cavopulmonary shunt:
853 mechanisms and clinical implications. *Expert Rev Cardiovasc Ther.* 2014;12(6):703-13.
854 7. Spearman AD, and Ginde S. Pulmonary Vascular Sequelae of Palliated Single Ventricle
855 Circulation: Arteriovenous Malformations and Aortopulmonary Collaterals. *Journal of*
856 *Cardiovascular Development and Disease.* 2022;9(9):309.
857 8. Shah MJ, Rychik J, Fogel MA, Murphy JD, and Jacobs ML. Pulmonary AV Malformations
858 After Superior Cavopulmonary Connection: Resolution After Inclusion of Hepatic Veins
859 in the Pulmonary Circulation. *The Annals of Thoracic Surgery.* 1997;63(4):960-3.
860 9. Kurotobi S, Sano T, Kogaki S, Matsushita T, Miwatani T, Takeuchi M, et al. Bidirectional
861 cavopulmonary shunt with right ventricular outflow patency: The impact of pulsatility
862 on pulmonary endothelial function. *The Journal of thoracic and cardiovascular surgery.*
863 2001;121(6):1161-8.
864 10. Henaine R, Vergnat M, Mercier O, Serraf A, De Montpreville V, Ninet J, et al.
865 Hemodynamics and arteriovenous malformations in cavopulmonary anastomosis: the
866 case for residual antegrade pulsatile flow. *The Journal of thoracic and cardiovascular*
867 *surgery.* 2013;146(6):1359-65.
868 11. Sakaki M, Taenaka Y, Tatsumi E, Nakatani T, Kinoshita M, Akagi H, et al. Pulmonary
869 function in a non-pulsatile pulmonary circulation. *ASAIO J.* 1992;38(3):M366-9.
870 12. Townsley MI. Structure and composition of pulmonary arteries, capillaries, and veins.
871 *Compr Physiol.* 2012;2(1):675-709.
872 13. Wetzel-Strong SE, Detter MR, and Marchuk DA. The pathobiology of vascular
873 malformations: insights from human and model organism genetics. *J Pathol.*
874 2017;241(2):281-93.
875 14. Chen W, Guo Y, Walker EJ, Shen F, Jun K, Oh SP, et al. Reduced mural cell coverage and
876 impaired vessel integrity after angiogenic stimulation in the Alk1-deficient brain.
877 *Arterioscler Thromb Vasc Biol.* 2013;33(2):305-10.
878 15. Brahmbhatt A, Remuzzi A, Franzoni M, and Misra S. The molecular mechanisms of
879 hemodialysis vascular access failure. *Kidney Int.* 2016;89(2):303-16.

880 16. Li Y, He Y, Falzon I, Fairbourn B, Tingey S, Imrey PB, et al. Dynamic Remodeling of
881 Human Arteriovenous Fistula Wall Obtained From Magnetic Resonance Imaging
882 During the First 6 Months After Creation. *Kidney Int Rep.* 2022;7(8):1905-9.
883 17. Corada M, Morini MF, and Dejana E. Signaling pathways in the specification of arteries
884 and veins. *Arterioscler Thromb Vasc Biol.* 2014;34(11):2372-7.
885 18. Peng T, Tian Y, Boogerd CJ, Lu MM, Kadzik RS, Stewart KM, et al. Coordination of heart
886 and lung co-development by a multipotent cardiopulmonary progenitor. *Nature.*
887 2013;500(7464):589-92.
888 19. Schwarz MA, and Cleaver OB. *The Pulmonary Endothelium*. 2009:1-24.
889 20. Buschmann I, Pries A, Styp-Rekowska B, Hillmeister P, Loufrani L, Henrion D, et al.
890 Pulsatile shear and Gja5 modulate arterial identity and remodeling events during flow-
891 driven arteriogenesis. *Development.* 2010;137(13):2187-96.
892 21. Dessalles CA, Leclech C, Castagnino A, and Barakat AI. Integration of substrate- and
893 flow-derived stresses in endothelial cell mechanobiology. *Commun Biol.* 2021;4(1):764.
894 22. McEvoy E, Sneh T, Moeendarbary E, Javanmardi Y, Efimova N, Yang C, et al. Feedback
895 between mechanosensitive signaling and active forces governs endothelial junction
896 integrity. *Nat Commun.* 2022;13(1):7089.
897 23. Kutys ML, and Chen CS. Forces and mechanotransduction in 3D vascular biology. *Curr*
898 *Opin Cell Biol.* 2016;42:73-9.
899 24. Baeyens N, Bandyopadhyay C, Coon BG, Yun S, and Schwartz MA. Endothelial fluid
900 shear stress sensing in vascular health and disease. *J Clin Invest.* 2016;126(3):821-8.
901 25. Jufri NF, Mohamedali A, Avolio A, and Baker MS. Mechanical stretch: physiological and
902 pathological implications for human vascular endothelial cells. *Vasc Cell.* 2015;7:8.
903 26. Mierke CT. Mechanosensory entities and functionality of endothelial cells. *Front Cell*
904 *Dev Biol.* 2024;12:1446452.
905 27. Zhao S, Suciu A, Ziegler T, Moore JE, Jr., Burki E, Meister JJ, et al. Synergistic effects of
906 fluid shear stress and cyclic circumferential stretch on vascular endothelial cell
907 morphology and cytoskeleton. *Arterioscler Thromb Vasc Biol.* 1995;15(10):1781-6.
908 28. Russo TA, Banuth AMM, Nader HB, and Dreyfuss JL. Altered shear stress on endothelial
909 cells leads to remodeling of extracellular matrix and induction of angiogenesis. *PLoS*
910 *One.* 2020;15(11):e0241040.
911 29. Wasserman SM, and Topper JN. Adaptation of the endothelium to fluid flow: in vitro
912 analyses of gene expression and in vivo implications. *Vasc Med.* 2004;9(1):35-45.
913 30. Wang Y, Cao W, Cui J, Yu Y, Zhao Y, Shi J, et al. Arterial Wall Stress Induces Phenotypic
914 Switching of Arterial Smooth Muscle Cells in Vascular Remodeling by Activating the
915 YAP/TAZ Signaling Pathway. *Cell Physiol Biochem.* 2018;51(2):842-53.
916 31. Lindahl P, Johansson BR, Leveen P, and Betsholtz C. Pericyte loss and microaneurysm
917 formation in PDGF-B-deficient mice. *Science.* 1997;277(5323):242-5.
918 32. Hellstrom M, Kalen M, Lindahl P, Abramsson A, and Betsholtz C. Role of PDGF-B and
919 PDGFR-beta in recruitment of vascular smooth muscle cells and pericytes during
920 embryonic blood vessel formation in the mouse. *Development.* 1999;126(14):3047-55.
921 33. Nadeem T, Bogue W, Bigit B, and Cuervo H. Deficiency of Notch signaling in pericytes
922 results in arteriovenous malformations. *JCI Insight.* 2020;5(21).
923 34. Lin Y, Gahn J, Banerjee K, Dobreva G, Singhal M, Dubrac A, et al. Role of endothelial
924 PDGFB in arterio-venous malformations pathogenesis. *Angiogenesis.* 2024;27(2):193-
925 209.

926 35. Uebelhoer M, Natynki M, Kangas J, Mendola A, Nguyen HL, Soblet J, et al. Venous
927 malformation-causative TIE2 mutations mediate an AKT-dependent decrease in
928 PDGFB. *Hum Mol Genet.* 2013;22(17):3438-48.
929 36. Wan TC, Rousseau H, Mattern C, Tabor M, Hodges MR, Ramchandran R, et al. Glenn
930 circulation causes early and progressive shunting in a surgical model of pulmonary
931 arteriovenous malformations. *Physiol Rep.* 2024;12(22):e70123.
932 37. Deng H, Eichmann A, and Schwartz MA. Fluid Shear Stress-Regulated Vascular
933 Remodeling: Past, Present, and Future. *Arterioscler Thromb Vasc Biol.* 2025.
934 38. Gaddis N, Fortriede J, Guo M, Bardes EE, Kouril M, Tabar S, et al. LungMAP Portal
935 Ecosystem: Systems-level Exploration of the Lung. *Am J Respir Cell Mol Biol.*
936 2024;70(2):129-39.
937 39. Guo M, Morley MP, Jiang C, Wu Y, Li G, Du Y, et al. Guided construction of single cell
938 reference for human and mouse lung. *Nat Commun.* 2023;14(1):4566.
939 40. Resnick N, Collins T, Atkinson W, Bonthron DT, Dewey CF, Jr., and Gimbrone MA, Jr.
940 Platelet-derived growth factor B chain promoter contains a cis-acting fluid shear-
941 stress-responsive element. *Proc Natl Acad Sci U S A.* 1993;90(10):4591-5.
942 41. Zerwes HG, and Risau W. Polarized secretion of a platelet-derived growth factor-like
943 chemotactic factor by endothelial cells in vitro. *J Cell Biol.* 1987;105(5):2037-41.
944 42. Yuliana ME, Huang ZH, Chou HC, and Chen CM. Effects of uteroplacental insufficiency
945 on growth-restricted rats with altered lung development: A metabolomic analysis.
946 *Front Pediatr.* 2022;10:952313.
947 43. McFaul RC, Tajik AJ, Mair DD, Danielson GK, and Seward JB. Development of pulmonary
948 arteriovenous shunt after superior vena cava-right pulmonary artery (Glenn)
949 anastomosis. Report of four cases. *Circulation.* 1977;55(1):212-6.
950 44. Cloutier A, Ash JM, Smallhorn JF, Williams WG, Trusler GA, Rowe RD, et al. Abnormal
951 distribution of pulmonary blood flow after the Glenn shunt or Fontan procedure: risk
952 of development of arteriovenous fistulae. *Circulation.* 1985;72(3):471-9.
953 45. Gray RG, Altmann K, Mosca RS, Prakash A, Williams IA, Quaegebeur JM, et al. Persistent
954 antegrade pulmonary blood flow post-glenn does not alter early post-Fontan outcomes
955 in single-ventricle patients. *Ann Thorac Surg.* 2007;84(3):888-93; discussion 93.
956 46. Chen Q, Tulloh R, Caputo M, Stoica S, Kia M, and Parry AJ. Does the persistence of
957 pulsatile antegrade pulmonary blood flow following bidirectional Glenn procedure
958 affect long term outcome? *Eur J Cardiothorac Surg.* 2015;47(1):154-8; discussion 8.
959 47. Kowatari R, Suzuki Y, Daitoku K, and Fukuda I. Long-term results of additional
960 pulmonary blood flow with bidirectional cavopulmonary shunt. *J Cardiothorac Surg.*
961 2020;15(1):279.
962 48. Berdat PA, Belli E, Lacour-Gayet F, Planche C, and Serraf A. Additional pulmonary blood
963 flow has no adverse effect on outcome after bidirectional cavopulmonary anastomosis.
964 *Ann Thorac Surg.* 2005;79(1):29-36; discussion -7.
965 49. van de Wal HJCM, Ouknine R, Tamisier D, Lévy M, Vouhé PR, and Leca F. Bi-directional
966 cavopulmonary shunt: is accessory pulsatile flow, good or bad? *European Journal of*
967 *Cardio-Thoracic Surgery.* 1999;16(2):104-10.
968 50. Ferns SJ, El Zein C, Multani K, Sajan I, Subramanian S, Polimenakos AC, et al. Is
969 additional pulsatile pulmonary blood flow beneficial to patients with bidirectional
970 Glenn? *The Journal of thoracic and cardiovascular surgery.* 2013;145(2):451-4.

971 51. Uemura H, Yagihara T, Kawashima Y, Okada K, Kamiya T, and Anderson RH. Use of the
972 bidirectional Glenn procedure in the presence of forward flow from the ventricles to
973 the pulmonary arteries. *Circulation.* 1995;92(9 Suppl):II228-32.
974 52. Januszewska K, Nawrocki P, Bruenen A, Schnabel A, and Malec E. Significance of
975 additional pulmonary blood flow between second and third stage in Fontan pathway.
976 *BMC pediatrics.* 2024;24(1):705.
977 53. Lammers S, Scott D, Hunter K, Tan W, Shandas R, and Stenmark KR. *Comprehensive*
978 *Physiology*. 2012:295-319.
979 54. Sumpio BE, Du W, Galagher G, Wang X, Khachigian LM, Collins T, et al. Regulation of
980 PDGF-B in endothelial cells exposed to cyclic strain. *Arterioscler Thromb Vasc Biol.*
981 1998;18(3):349-55.
982 55. Kolpakov V, Rekhter MD, Gordon D, Wang WH, and Kulik TJ. Effect of mechanical forces
983 on growth and matrix protein synthesis in the in vitro pulmonary artery. Analysis of
984 the role of individual cell types. *Circ Res.* 1995;77(4):823-31.
985 56. Lin C, Zheng X, Lin S, Zhang Y, Wu J, and Li Y. Mechanotransduction Regulates the
986 Interplays Between Alveolar Epithelial and Vascular Endothelial Cells in Lung. *Front*
987 *Physiol.* 2022;13:818394.
988 57. R RF, Fukui H, Chow R, Vilfan A, and Vermot J. The cilium as a force sensor-myth versus
989 reality. *J Cell Sci.* 2019;132(14).
990 58. Spurgin S, Nguimtsop AM, Chaudhry FN, Michki SN, Salvador J, Iruela-Arispe ML, et al.
991 Dynamics of primary cilia in endothelial and mesenchymal cells throughout mouse
992 lung development. *Dev Dyn.* 2025;254(11):1187-202.
993 59. Tanaka K, Chen M, Prendergast A, Zhuang Z, Nasiri A, Joshi D, et al. Latrophilin-2
994 mediates fluid shear stress mechanotransduction at endothelial junctions. *EMBO J.*
995 2024;43(15):3175-91.
996 60. Van Gieson EJ, Murfee WL, Skalak TC, and Price RJ. Enhanced Smooth Muscle Cell
997 Coverage of Microvessels Exposed to Increased Hemodynamic Stresses In Vivo.
998 *Circulation Research.* 2003;92(8):929-36.
999 61. Singh E, Redgrave RE, Phillips HM, and Arthur HM. Arterial endoglin does not protect
1000 against arteriovenous malformations. *Angiogenesis.* 2020;23(4):559-66.
1001 62. Lee HW, Xu Y, He L, Choi W, Gonzalez D, Jin SW, et al. Role of Venous Endothelial Cells
1002 in Developmental and Pathologic Angiogenesis. *Circulation.* 2021;144(16):1308-22.
1003 63. Wang JH, Goldschmidt-Clermont P, Wille J, and Yin FC. Specificity of endothelial cell
1004 reorientation in response to cyclic mechanical stretching. *J Biomech.*
1005 2001;34(12):1563-72.
1006 64. Takeda R, Yamaguchi T, Hayashi S, Sano S, Kawame H, Kanki S, et al. Clinical and
1007 molecular features of patients with COL1-related disorders: Implications for the wider
1008 spectrum and the risk of vascular complications. *Am J Med Genet A.* 2022;188(9):2560-
1009 75.
1010 65. Lesnik P, Haskell CA, and Charo IF. Decreased atherosclerosis in CX3CR1−/− mice
1011 reveals a role for fractalkine in atherogenesis. *Journal of Clinical Investigation.*
1012 2003;111(3):333-40.
1013 66. Bazan JF, Bacon KB, Hardiman G, Wang W, Soo K, Rossi D, et al. A new class of
1014 membrane-bound chemokine with a CX3C motif. *Nature.* 1997;385(6617):640-4.
1015 67. Chen Y, Zhu W, Bollen AW, Lawton MT, Barbaro NM, Dowd CF, et al. Evidence of
1016 Inflammatory Cell Involvement in Brain Arteriovenous Malformations. *Neurosurgery.*
1017 2008;62(6):1340-50.

1018 68. Zhang R, Han Z, Degos V, Shen F, Choi EJ, Sun Z, et al. Persistent infiltration and pro-
1019 inflammatory differentiation of monocytes cause unresolved inflammation in brain
1020 arteriovenous malformation. *Angiogenesis.* 2016;19(4):451-61.
1021 69. Braverman IM, Keh A, and Jacobson BS. Ultrastructure and three-dimensional
1022 organization of the telangiectases of hereditary hemorrhagic telangiectasia. *J Invest*
1023 *Dermatol.* 1990;95(4):422-7.
1024 70. Kim SJ, Bae EJ, Cho DJ, Park IS, Kim YM, Kim W-H, et al. Development of pulmonary
1025 arteriovenous fistulas after bidirectional cavopulmonary shunt. *The Annals of Thoracic*
1026 *Surgery.* 2000;70(6):1918-22.
1027 71. Vettukattil JJ, Slavik Z, Lamb RK, Monro JL, Keeton BR, Tsang VT, et al. Intrapulmonary
1028 arteriovenous shunting may be a universal phenomenon in patients with the superior
1029 cavopulmonary anastomosis: a radionuclide study. *Heart (British Cardiac Society).*
1030 2000;83(4):425-8.
1031 72. Feinstein JA, Moore P, Rosenthal DN, Puchalski M, and Brook MM. Comparison of
1032 contrast echocardiography versus cardiac catheterization for detection of pulmonary
1033 arteriovenous malformations. *The American journal of cardiology.* 2002;89(3):281-5.
1034 73. Stoller JKH, Robert M.
1035 White, Richard D., and Mee RB. Anomalous Hepatic Venous Drainage into the Left Atrium: An
1036 Unusual Cause of Hypoxemia. *Respiratory Care.* 2003;48(1):58-62.
1037 74. Guardado FJ, Byrd TM, and Petersen WG. Azygous continuation of the inferior vena
1038 cava with anomalous hepatic vein drainage. *Am J Med Sci.* 2012;343(3):259-61.
1039 75. Lee J, Menkis AH, and Rosenberg HC. Reversal of pulmonary arteriovenous
1040 malformation after diversion of anomalous hepatic drainage. *Ann Thorac Surg.*
1041 1998;65(3):848-9.
1042 76. Kloppenburg GT, Post MC, Mager HJ, and Schepens MA. Rerouting anomalous hepatic
1043 venous connection to the left atrium. *Ann Thorac Surg.* 2010;90(2):638-40.
1044 77. Yim D, Nagata H, Lam CZ, Grosse-Wortmann L, Seed M, Jaeggi E, et al. Disharmonious
1045 Patterns of Heterotaxy and Isomerism: How Often Are the Classic Patterns Breached?
1046 *Circ Cardiovasc Imaging.* 2018;11(2):e006917.
1047 78. Duncan BW, Kneebone JM, Chi EY, Hraska V, Isik FF, Rosenthal GL, et al. A detailed
1048 histologic analysis of pulmonary arteriovenous malformations in children with
1049 cyanotic congenital heart disease. *The Journal of thoracic and cardiovascular surgery.*
1050 1999;117(5):931-8.
1051 79. Starnes SL, Duncan BW, Kneebone JM, Fraga CH, States S, Rosenthal GL, et al.
1052 Pulmonary microvessel density is a marker of angiogenesis in children after
1053 cavopulmonary anastomosis. *The Journal of thoracic and cardiovascular surgery.*
1054 2000;120(5):902-8.
1055 80. Starnes SL, Duncan BW, Fraga CH, Desai SY, Jones TK, Mathur SK, et al. Rat model of
1056 pulmonary arteriovenous malformations after right superior cavopulmonary
1057 anastomosis. *Am J Physiol Heart Circ Physiol.* 2002;283(5):H2151-6.
1058 81. Hays BS, Baker M, Laib A, Tan W, Udholm S, Goldstein BH, et al. Histopathological
1059 abnormalities in the central arteries and veins of Fontan subjects. *Heart (British*
1060 *Cardiac Society).* 2018;104(4):324-31.
1061 82. Ridderbos FJ, Wolff D, Timmer A, van Melle JP, Ebels T, Dickinson MG, et al. Adverse
1062 pulmonary vascular remodeling in the Fontan circulation. *J Heart Lung Transplant.*
1063 2015;34(3):404-13.

1064 83. Velasco Forte MN, Roujol S, Ruijsink B, Valverde I, Duong P, Byrne N, et al. MRI for
1065 Guided Right and Left Heart Cardiac Catheterization: A Prospective Study in Congenital
1066 Heart Disease. *J Magn Reson Imaging.* 2021;53(5):1446-57.
1067 84. Lord SJ, Velle KB, Mullins RD, and Fritz-Laylin LK. SuperPlots: Communicating
1068 reproducibility and variability in cell biology. *J Cell Biol.* 2020;219(6).
1069
1070

Figures

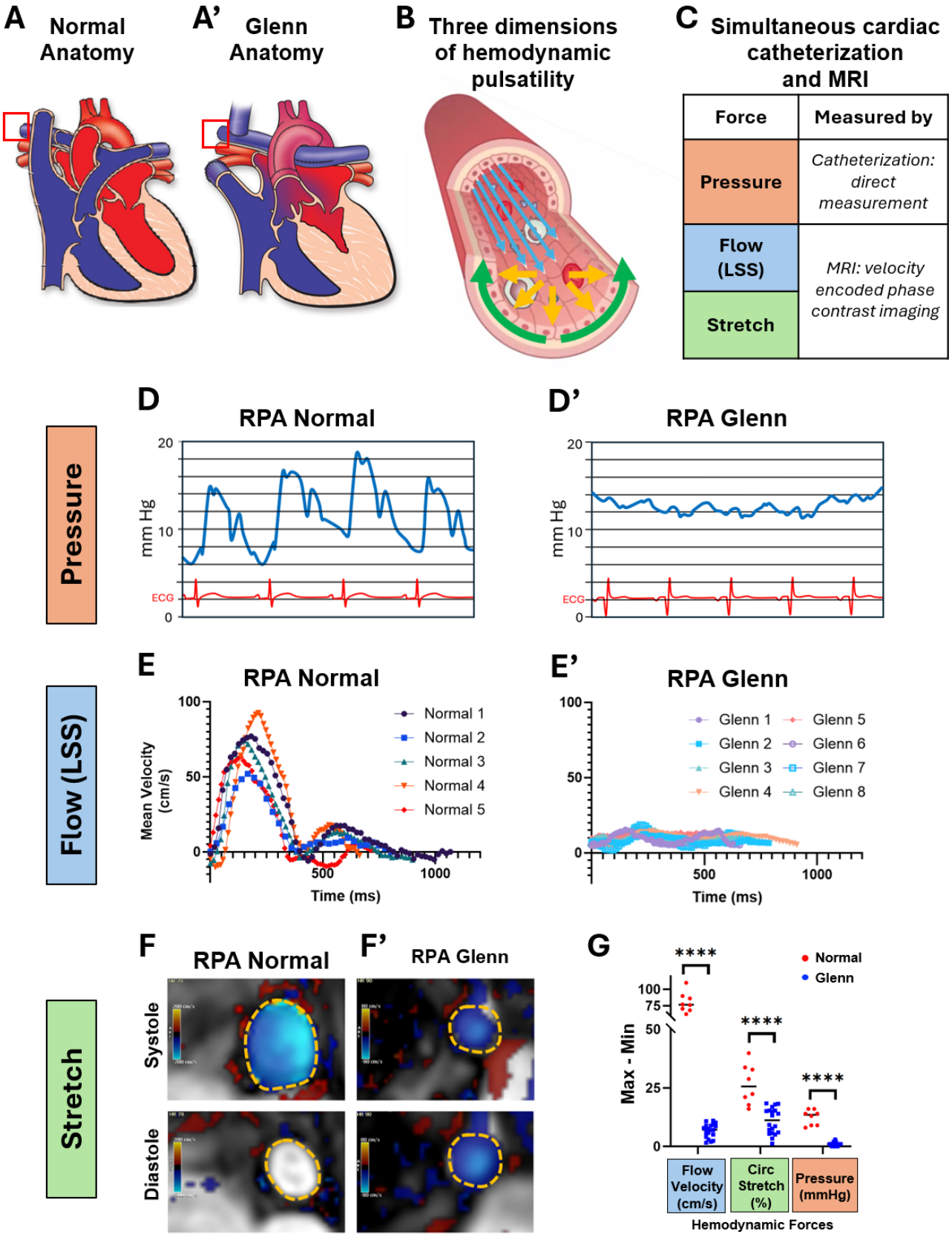
A
Normal Anatomy
A'
Glenn Anatomy
B
Three dimensions of hemodynamic pulsatility
C
Simultaneous cardiac catheterization and MRI
Force
Measured by
Pressure
Catheterization: direct measurement
Flow (LSS)
Stretch
MRI: velocity encoded phase contrast imaging
Pressure
D
RPA Normal
D'
RPA Glenn
mm Hg
ECG
Flow (LSS)
E
RPA Normal
E'
RPA Glenn
Mean Velocity (cm/s)
Time (ms)
Normal 1
Normal 2
Normal 3
Normal 4
Normal 5
Glenn 1
Glenn 2
Glenn 3
Glenn 4
Glenn 5
Glenn 6
Glenn 7
Glenn 8
Stretch
F
RPA Normal
F'
RPA Glenn
Systole
Diastole
G
Normal
Glenn
Max - Min
****
Flow Velocity (cm/s)
Circ Stretch (%)
Pressure (mmHg)
Hemodynamic Forces

730 **Figure 1. Loss of pulsatility in three dimensions within Glenn pulmonary arteries.**
731 **(A, A')** Diagrams of representative normal and Glenn cardiopulmonary anatomy. Red
732 box highlights location of force pulsatility measurements. **(B)** Hemodynamic forces act
733 on ECs in three dimensions: shear/flow (blue), pressure (orange), and circumferential
734 stretch (green). (Schematic adapted from graphic on Ibidi.com). **(C)** Outline of data
735 collection method for each dimension of hemodynamic force. **(D, D')** Example pressure
736 waveforms from the right pulmonary artery of normal and Glenn patients.
737 Electrocardiogram shown in red for correlation to cardiac cycle. RPA, right pulmonary
738 artery. **(E, E')** Variation in flow velocity of the proximal right pulmonary artery measured
739 by cardiac MRI throughout a cardiac cycle from systole (start) to end-diastole (end).
740 Variability in length of time for each patient reflects the variable heart rate within each
741 subject. **(F, F')** Cardiac MRI velocity encoded phase contrast images with color showing
742 velocity of blood flow out of the plane of the image slice. Dotted orange line shows RPA
743 border. RPA diameter increases during systole in anormal patients but does not
744 increase during systole in Glenn patient. **(G)** Quantification of pulse difference of each
745 dimension of force, obtained during combined cardiac catheterization and cardiac MRI
746 of normal (n=20) and Glenn (n=20) patients, demonstrating loss of pulsatility in the
747 Glenn. Circumference % change is calculated from baseline in diastole.
748
749

A **Applying pulsatility to ECs in isolated dimensions of force**

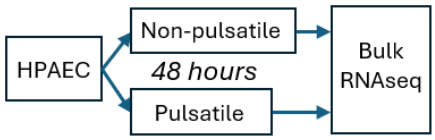

	Non-Pulsatile	Pulsatile
Flow	15 dyn/cm^2	0-15 dyn/cm^2 1 Hz
Pressure	25 mm Hg	5-25 mm Hg 1 Hz
Stretch	0%	10% 1 Hz

B

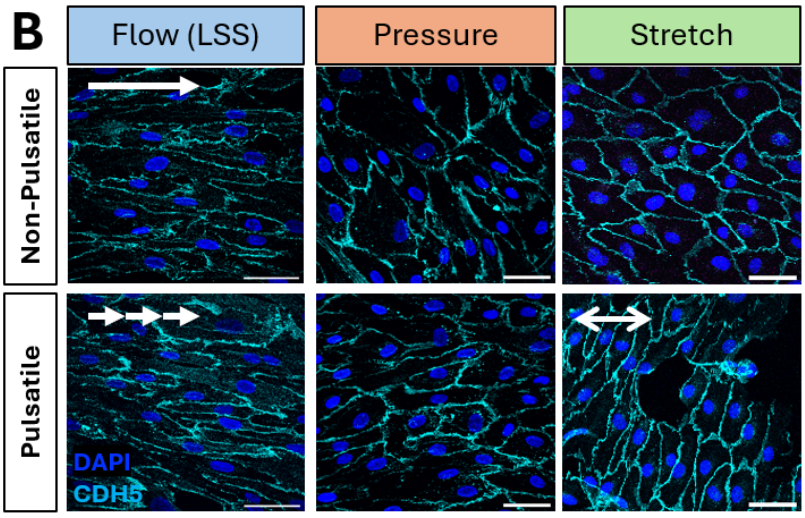

C **Regulated Pathways: Pulsatile [Force] vs Non-pulsatile [Force]**

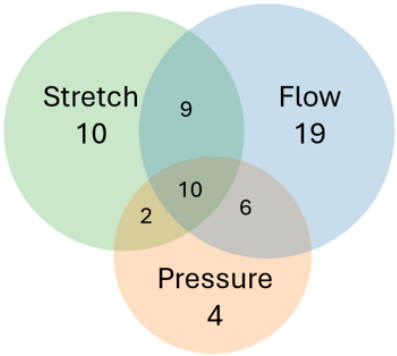

D

E **Contributions to KEGG pathway: regulation of actin cytoskeleton**

Pulsatile Force	Selected Contributors
Flow (LSS)	*Rac2, Map2k1, Myl12a, Pdgfb*
Pressure	*Itga6, Rac3, Cdc42, Actn1*
Stretch	*Actn4, Itga3, Arghef6, Pdgfb*

750

751 **Figure 2. Pulsatility drives both similar and distinct signaling pathways within**
752 **each dimension of force. (A)** Experimental conditions: HPAECs were exposed to 48
753 hours of a single dimension of either non-pulsatile or pulsatile force, and bulk RNA
754 sequencing was performed. **(B)** GSEA of bulk RNAseq data shows overlapping and
755 unique pathways activated by each dimension of force. **(C)** Representative images of
756 the cell-shape adjustments that occur in response to the different forces are shown. **(D)**
757 Normalized enrichment score (NES) and adjusted p-value (adj p-val) shown for select
758 signaling pathways shows greater impact of pulsatility within flow and stretch relative to
759 pulsatility of pressure. **(E)** Key genes with the actin cytoskeleton pathway that are
760 upregulated by each dimension of force. **(F)** *Pdgfb* was downregulated in 11 of
761 dysregulated pathways identified in E.
762

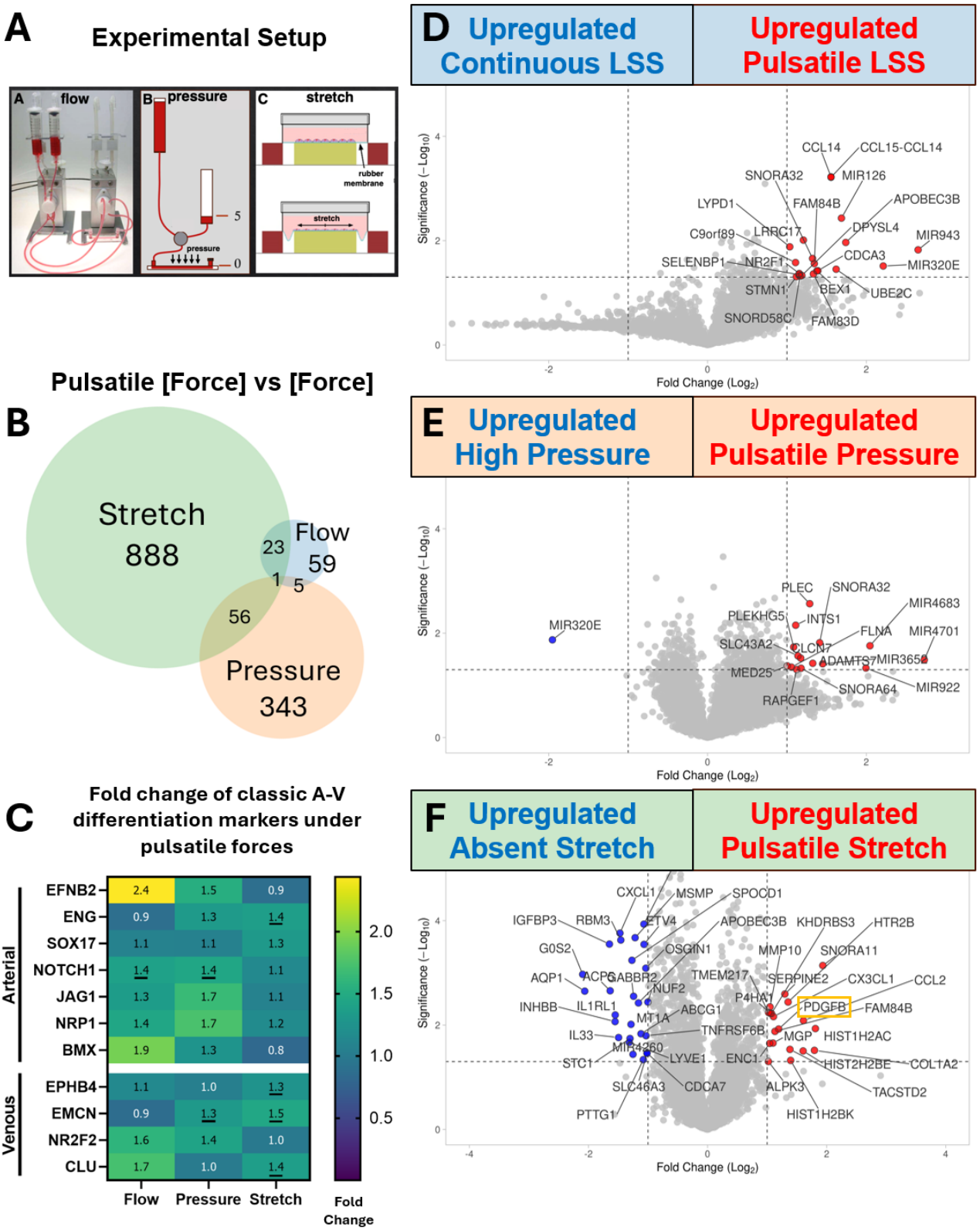

763

764 **Figure 3. Impact of pulsatile stretch is greater than pulsatile pressure or flow but**

765 **does not change classical arteriovenous differentiation. (A)** Diagram of cell culture

766 setup to apply isolated dimensions of force to ECs. **(B)** Venn diagram of the number of
767 genes significantly up- or down-regulated by pulsatility of flow, pressure, or stretch. **(C)**
768 Fold change (pulsatile/non-pulsatile) of any classic EC arteriovenous differentiation
769 markers by bulk RNAseq. Color scale denotes fold change, exact number in each box.
770 Significant changes (p-values < 0.05) are underlined. **(D-F)** Volcano plots of significantly
771 regulated genes within each dimension of pulsatile force: **(D)** LSS; **(E)** pressure; and **(F)**
772 stretch.
773
774

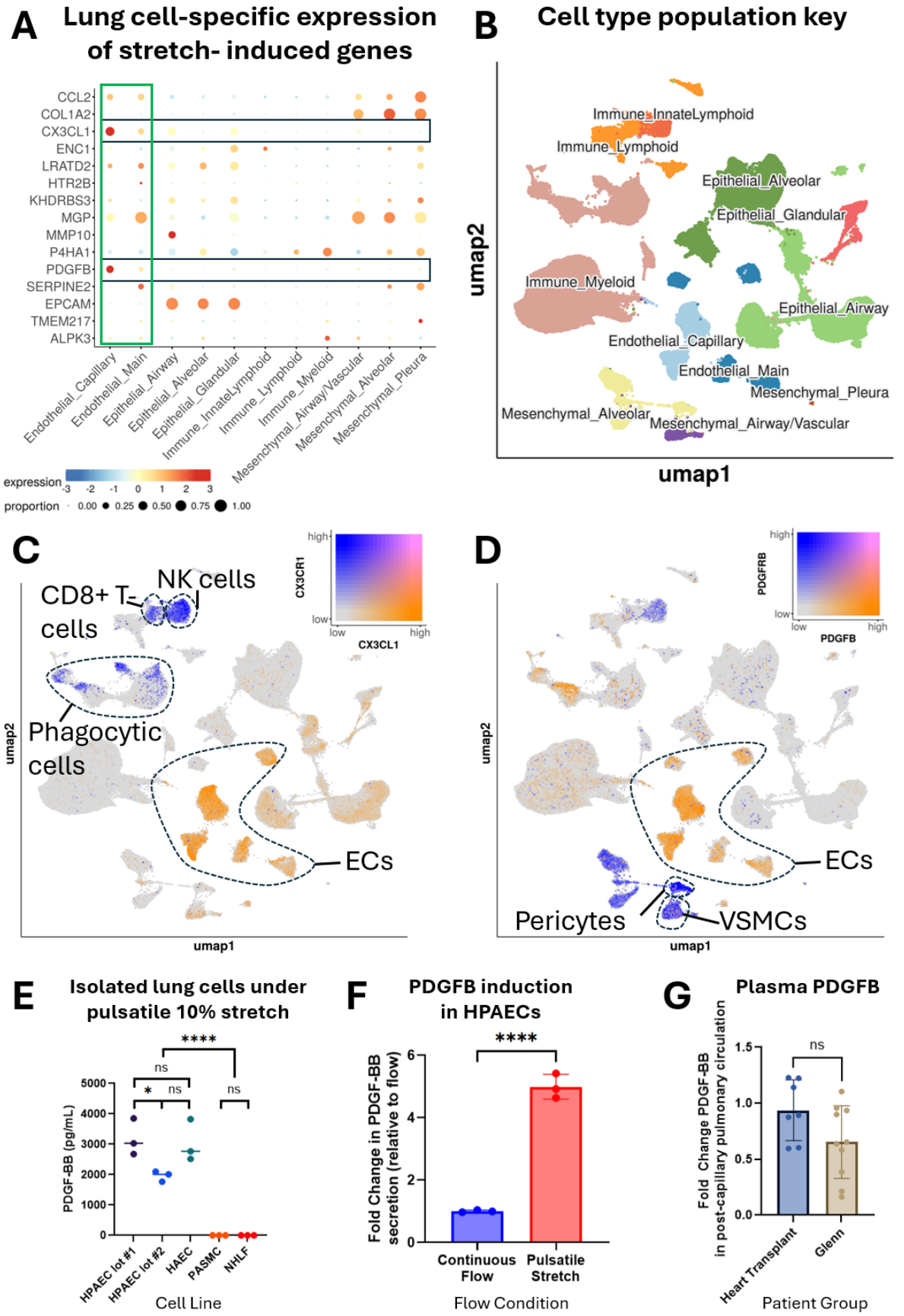
A
Lung cell-specific expression of stretch- induced genes
CCL2
COL1A2
CX3CL1
ENC1
LRATD2
HTR2B
KHDRBS3
MGP
MMP10
P4HA1
PDGFB
SERPINE2
EPCAM
TMEM217
ALPK3
Endothelial_Capillary
Endothelial_Main
Epithelial_Airway
Epithelial_Alveolar
Epithelial_Glandular
Immune_InnateLymphoid
Immune_Lymphoid
Immune_Myeloid
Mesenchymal_Airway/Vascular
Mesenchymal_Alveolar
Mesenchymal_Pleura
expression
-3 -2 -1 0 1 2 3
proportion
0.00 0.25 0.50 0.75 1.00
B
Cell type population key
Immune_InnateLymphoid
Immune_Lymphoid
Epithelial_Alveolar
Epithelial_Glandular
Immune_Myeloid
Epithelial_Airway
Endothelial_Capillary
Endothelial_Main
Mesenchymal_Pleura
Mesenchymal_Alveolar
Mesenchymal_Airway/Vascular
umap2
umap1
C
CD8+ T-cells
NK cells
Phagocytic cells
ECs
CX3CR1
CX3CL1
high
low
umap2
umap1
D
PDGFRB
PDGFB
high
low
ECs
Pericytes
VSMCs
umap2
umap1
E
Isolated lung cells under pulsatile 10% stretch
PDGF-BB (pg/mL)
5000
4000
3000
2000
1000
0
****
ns
*
ns
ns
HPAEC lot #1
HPAEC lot #2
HAEC
PASMC
NHLF
Cell Line
F
PDGFB induction in HPAECs
Fold Change in PDGF-BB secretion (relative to flow)
6
4
2
0
****
Continuous Flow
Pulsatile Stretch
Flow Condition
G
Plasma PDGFB
Fold Change PDGF-BB in post-capillary pulmonary circulation
1.5
1.0
0.5
0.0
ns
Heart Transplant
Glenn
Patient Group

775

776 **Figure 4. PDGFB expression in human lungs is endothelial-specific and stretch-**
777 **induced. (A)** Genes upregulated by pulsatile stretch in ECs were analyzed within the
778 LungMAP single cell RNA sequencing data of human lung tissue (347,970 cells).
779 Expression within ECs (green box) was compared to other cell types. CX3CL1 and
780 PDGFB (black boxes) were uniquely expressed by ECs. **(B)** Cell population groupings
781 as annotated by LungMAP cell x gene portal. **(C)** Gene co-expression analysis shows
782 expression of *Cx3cl1* in ECs with its receptor *Cx3cr1* in immune cells. **(D)** Expression of
783 *Pdgfb* is high in ECs, with its receptor *Pdgfrb* found in pericytes and vascular smooth
784 muscle. **(E)** Different cell lines comprising the primary components of a blood vessel
785 (endothelium, smooth muscle, fibroblasts) were exposed to pulsatile uniaxial 10%
786 stretch at 1 Hz and only ECs secreted PDGFB into the media (as measured by ELISA).
787 **(F)** Pulsatile stretch of cultured HPAECs induces 5x more PDGFB secretion than
788 continuous flow. Error bar shows 1 s.d. **(G)** PDGFB measured by ELISA from patient
789 plasma does not show a significant arteriovenous concentration gradient or difference
790 between normal and Glenn patients. Error bar shows 1 s.d.
791
792

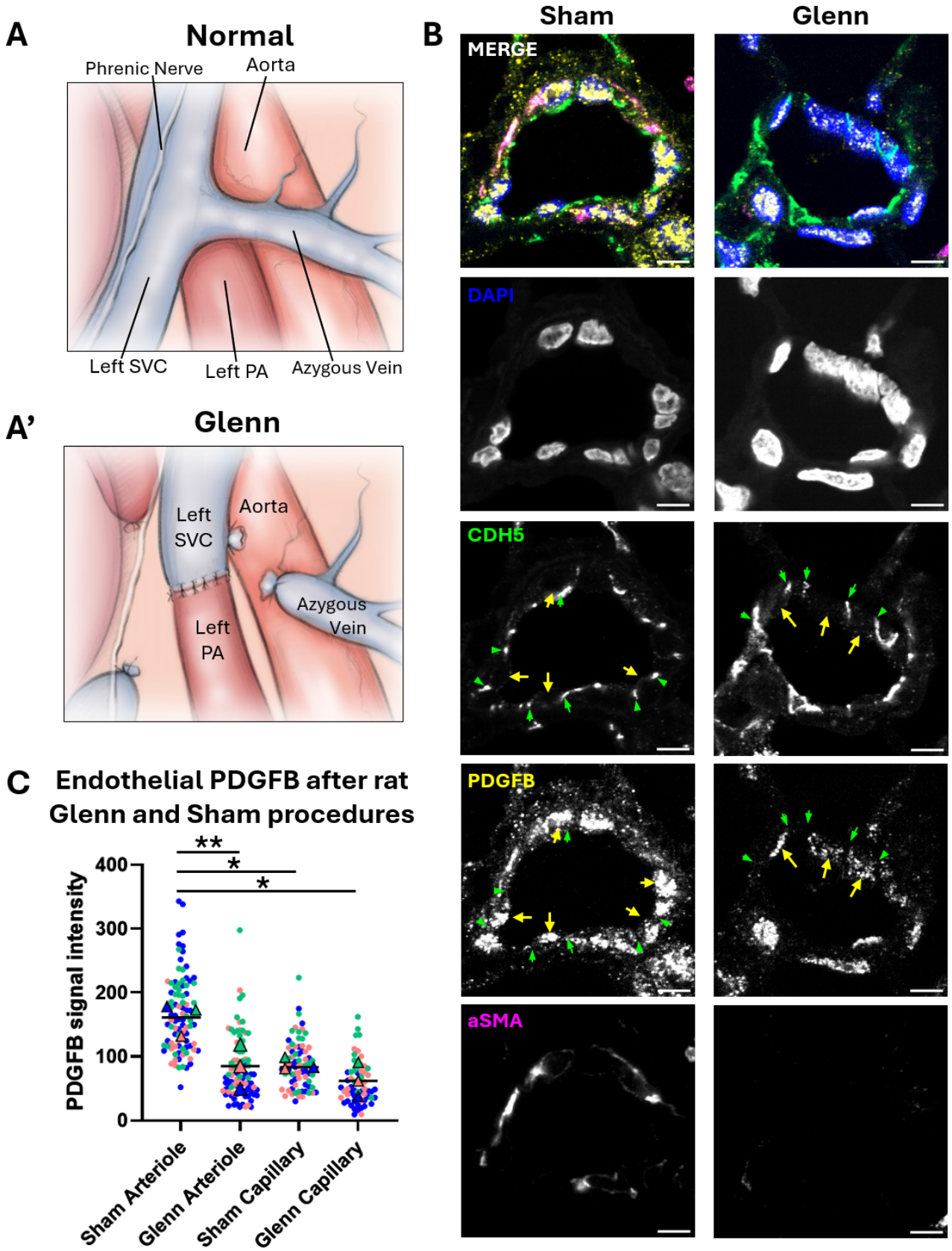
A
Normal
Phrenic Nerve
Aorta
Left SVC
Left PA
Azygous Vein
A'
Glenn
Left SVC
Aorta
Azygous Vein
Left PA
B
Sham
Glenn
MERGE
DAPI
CDH5
PDGFB
aSMA
C
Endothelial PDGFB after rat Glenn and Sham procedures
PDGFB signal intensity
400
300
200
100
0
**
*
*
Sham Arteriole
Glenn Arteriole
Sham Capillary
Glenn Capillary

793

794 **Figure 5. Loss of PDGFB in pulmonary endothelium of rats after Glenn surgery. (A)**
795 Schematic of normal rat vascular anatomy and (**A'**) rat Glenn surgery (adapted from Wan
796 2024 with permission). **(B)** Representative immunofluorescent (IF) staining of pulmonary
797 arterioles from left lung of sham and Glenn-operated rats. Pulmonary arterioles were
798 identified by presence of VECAD (cyan) and SMA (pink), near lung periphery, and less
799 than 50 μm in diameter. Scale bar is 5 μm. **(C)** Quantification of PDGFB staining in
800 pulmonary arteriolar and capillary ECs in sham (N=91 arteriolar ECs, N=74 capillary ECs)
801 and Glenn-operated (N=89 arteriolar ECs, N=62 capillary ECs) rats demonstrates
802 significant loss of EC-derived PDGFB in the Glenn lung. 5 vessels each from the left lung
803 of 3 sham and 3 Glenn rats were analyzed.
804
805

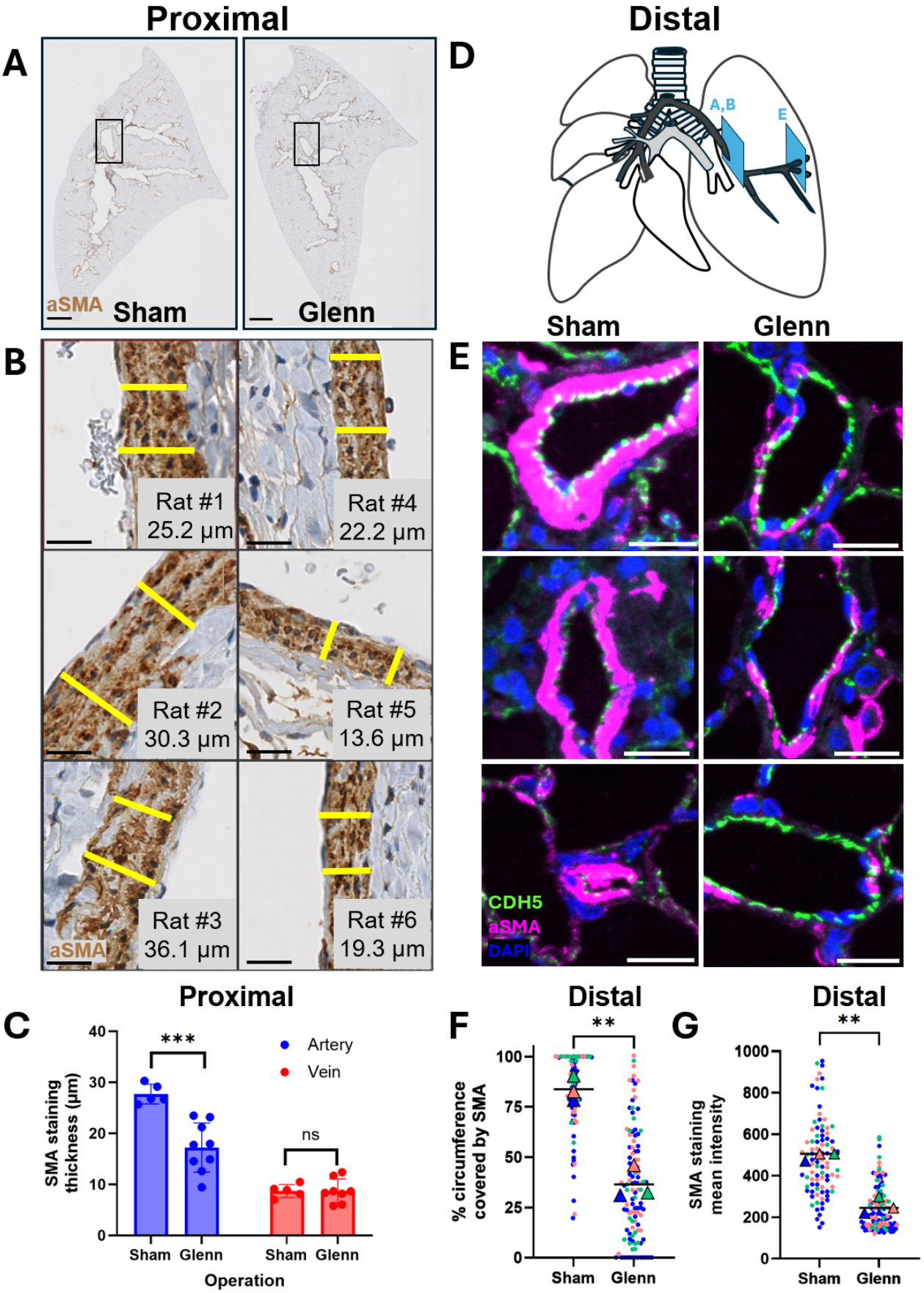
Proximal
A
aSMA
Sham
Glenn
Distal
D
A,B
E
B
Rat #1
25.2 µm
Rat #4
22.2 µm
Rat #2
30.3 µm
Rat #5
13.6 µm
Rat #3
36.1 µm
Rat #6
19.3 µm
aSMA
Sham
Glenn
E
CDH5
aSMA
DAPI
Proximal
C
SMA staining thickness (µm)
Artery
Vein
***
ns
Sham
Glenn
Sham
Glenn
Operation
Distal
F
% circumference covered by SMA
**
Sham
Glenn
Distal
G
SMA staining mean intensity
**
Sham
Glenn

806

807 **Figure 6. Loss of smooth muscle layer in pulmonary arteries of rats after Glenn**
808 **surgery. (A)** Example sagittal sections of lung tissue from sham and Glenn operated
809 rats, stained by IHC for smooth muscle actin (SMA). Black boxes show typical perihilar
810 location of analysis of the most proximal portions of pulmonary arteries examined. Scale
811 bar = 2 mm. **(B)** Left panels - Example images of SMA+ media thickness from 3
812 different sham operated rats. Scale bar = 20 μm. Right panels - Example images of
813 SMA+ media thickness from 3 different Glenn rats. Scale bar = 20 μm. **(C)**
814 Quantification of SMA+ tunica media from proximal arteries versus veins. **(D)** Schematic
815 showing approximate location of pulmonary vessels assayed in A, B and E. **(E)**
816 Examples of images of SMA+ media thickness in distal arterioles from 3 different sham
817 (left panels) and Glenn (right panels). Distal lung vessels < 0.1 mm were identified using
818 IF staining for CDH5 (green) in Sham (n=3 rats, n=42 vessels) and Glenn (n=3 rats,
819 n=56 vessels) rat lungs, and staining of SMA (pink) was used to quantify the
820 circumferential coverage **(F)** and intensity **(G) of** SMA surrounding these arterioles.
821

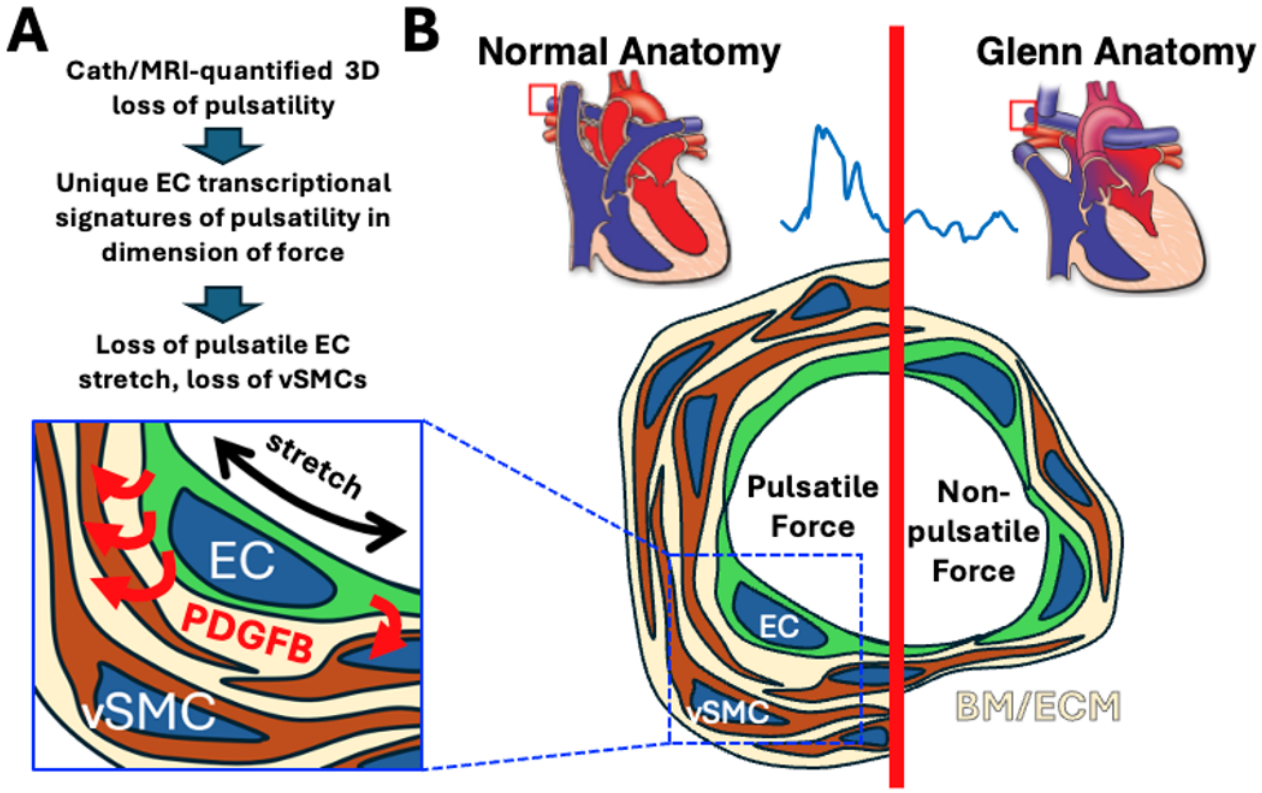

Figure 7. Outline of primary findings. **(A)** Overview of experimental results. **(B)** Comparison of findings between pulsatile and non-pulsatile conditions. Red boxes indicate region of pulmonary arteries analyzed in patients with either normal lung vascular architecture or Glenn anatomy. Blue box area shows increased PDGFB secretion from ECs following blood circulation-induced stretch. EC, endothelial cell (green); vSMC, vascular smooth muscle cell (brown); BM, basement membrane, and ECM; extracellular matrix (beige).